Alma Mater Studiorum · University of Bologna

School of Science
Department of Physics and Astronomy
Master Degree in Physics

Development of the Batcher Tool for the Optimization of the Batch Distribution

Univeristy Supervisor:
Prof. Paolo Finelli

Submitted by:
Lorenzo Barsotti

External Supervisors:
Dr. Francesco Lodi
Dr. Mattia Massone

Academic Year 2022/2023

Abstract

This thesis is the result of a 600-hours internship at ENEA. The objective of the internship was to develop an optimization algorithm aimed at determining the optimal distribution of fuel assemblies into *batches* within a nuclear reactor.

An optimal batch distribution meets certain criteria concerning reactivity and temperature distribution within the core map. Since the cooling and reactivity control systems must be dimensioned on a worst-case basis, it is necessary that all the cycles are as similar as possible.

We employed a *fitness* function based on the first-order perturbation theory to determine the goodness of a distribution. Knowing the perturbed cross-sections, which were provided as input, it was possible to calculate the variation from the reference states of the reactivity and a power functional in each phase of the cycle.

After the *fitness* function was defined, it was optimized by using two methods. The first is an analytical algorithm that attempts to minimize the nonlinear objective function by exploring the possible solutions through successive linearization to find the best solution. The second method is a genetic algorithm, based on natural selection processes, such as *cross-over*, *mutation* and *elitism*.

The two algorithms were applied to the test-case of ALFRED and the obtained results have been compared. In general, the analytical algorithm shows better results compared to the genetic one, both in terms of execution time and of the fitness function obtained. In any case, the results obtained from the two algorithms meet the requirements imposed during the modeling of the problem very well.

However, due to the algorithms' structure, it is expected that the choice of the best optimization algorithm will depend on the model of the problem to be solved. If the fitness function becomes very complicated, the computation of the analytical solution will take much longer, consequently making this method a worse choice.

Sommario

Questo lavoro di tesi è il frutto di un tirocinio di più di 600 ore svolto presso la divisione di Bologna di *Sicurezza e Sostenibilità Nucleare* dell'*Agenzia nazionale per le nuove tecnologie, l'energia e lo sviluppo economico sostenibile* (ENEA). Durante questo tirocinio è stato sviluppato un algoritmo di ottimizzazione per la ricerca della distribuzione in *batch* ottimale degli elementi di combustibile di un reattore nucleare. Una distribuzione in batch è considerata ottimale se soddisfa alcuni criteri fisico-ingegneristici riguardanti la reattività e la distribuzione di potenza all'interno della mappa di nocciolo. La prima deve essere costante tra i vari cicli del rifornimento di combustibile in quanto, siccome il sistema di controllo della reattività deve essere dimensionato sul caso peggiore, la soluzione ottimale è rendere tutte le fasi il più simile tra loro. Per quanto riguarda il secondo criterio, una distribuzione ottimale deve rispettare i limiti di temperatura imposti durante il design e, in particolare, quella della guaina che sostiene il combustibile che, in caso di superamento di tale temperatura limite, potrebbe essere corrosa dal piombo.

L'idea generale è quella di utilizzare una funzione di *fitness* per determinare la bontà di una distribuzione. Questa funzione è stata scritta sfruttando la teoria delle perturbazioni al primo ordine delle sezioni d'urto degli elementi. Le configurazioni in cui tutti gli elementi appartengono alla stessa *batch*, a inizio (BoC) e fine ciclo (EoC) sono state prese come riferimento. Conoscendo le sezioni d'urto negli istanti perturbati, che sono state fornite in *input*, è stato possibile calcolare la variazione della reattività e di un funzionale della potenza rispetto al caso di riferimento in ciascuna fase del ciclo.

Una volta definita la funzione di *fitness*, quest'ultima è stata ottimizzata, sfruttando due metodi indipendenti. Il primo consiste in un algoritmo di ottimizzazione analitica che cerca di minimizzare la (non lineare) funzione obiettivo esplorando le possibili soluzioni attraverso linearizzazioni successive e trovando la migliore soluzione. Il secondo metodo consiste, invece, in un algoritmo genetico, basato su processi di selezione naturale, come il *crossing-over*, le *mutazioni* e l'*elitismo*.

L'algoritmo sviluppato è stato poi applicato al caso test di un reattore nucleare dimostrativo raffreddato al piombo che verrà costruito in Romania nella prossima decade chiamato *Advanced Lead-cooled Fast Reactor European Demonstrator* (ALFRED).

Infine, i risultati ottenuti con i due metodi sono stati confrontati evidenziando, in generale, i migliori risultati dell'algoritmo analitico rispetto a quello genetico, sia in termini di tempo di esecuzione che di funzione di fitness ottenuta. In ogni caso, i risultati ottenuti dai due algoritmi hanno soddisfatto egregiamente le richieste imposte durante la modellazione del problema.

Nonostante ciò, per come sono strutturati i due algoritmi, ci si aspetta che la scelta del migliore algoritmo di ottimizzazione sia fortemente dipendente dal modello del problema da risolvere. In particolare, se la funzione di fitness diventa molto complicata rispetto al modello presente in questo lavoro di tesi, il computo della soluzione analitica, richiederà molto più tempo, rendendo di conseguenza questo metodo una scelta peggiore.

Contents

Chapter 1

Introduction

The world population is currently 8 billions, but it is expected to grow up to 10 billions by the end of the century [1]. The population growth is reflected in a growth in the demand of energy [2]. While increasing the quantity of renewable energy, such as solar and wind, in the energy mix is fundamental to reduce the carbon footprint, it is also crucial to remember that they cannot ensure a constant production of energy independently of external factors. In addition, nowadays, it is not possible to store easily large amount of energy. If this was possible, we could store the surplus of energy produced during windy and sunny days, and use it when we most need it. Another consideration about renewable energy sources is that the land consumption occupied by their structures can be up to 3 order of magnitude higher[1] compared to the land occupied by a nuclear power plant [3]. For these reasons, it is necessary to consider other forms of low carbon emission energy sources, such as nuclear energy.

On the other hand, existing nuclear reactors produce a small but not negligible quantity of radioactive waste that must be stored in special facilities for a period of time not comparable with the human lifespan. For this reason, there is the interest in technologies able to reduce the quantity, radiotoxicity, and the lifetime of high level radioactive waste produced during the working life of a nuclear reactor. This is one of the objective of the Generation IV reactors.

To achieve this goal, one of the most promising possibilities is to build fast reactor instead of traditional ones. That means that they work with a different neutrons energy with respect to most of the existing water reactors. This results in the possibility to close the fuel cycle and reduce the mean lifetime of the nuclear

[1] This is the case of onshore wind site, where we consider also the area between the turbines. For silicon photovoltaic, the land consumption is about one order of magnitude higher compared to a nuclear power plant.

waste, at the cost of a series of problematics that must be considered in the design of the reactor, such as the harsher operative conditions for the materials.

One of the reactors chosen to be the next generation of nuclear reactors is the Lead Fast Reactor (LFR), in which the coolant is either liquid lead or a lead-bismuth eutectic alloy. Most of the existing reactors have to be refuelled because, after the fuel depletion, the reactor is unable to deliver the desired amount of energy.

The refuelling process consists in the substitution with fresh elements of the fuel assemblies that have burned for the amount of time decided during the design process. As we will see in the next chapters, during refuelling not all the fuel assemblies in the core are substituted at once, but the process is split in phases, in which just a portion of the fuel assemblies is substituted each time, until all the fuel assemblies in the core have been replaced. Once this cycle ends, it is repeated: the first group of fuel assemblies that have been substituted, now have spent the target time in the core and must be refuelled again. Each group of fuel assemblies is called *batch*. For safety and efficiency reasons that will be discussed in the following chapters, the batch distribution (i.e. which fuel assembly belongs to which groups), must be chosen accordingly to some parameters. The most important ones are the *reactivity* and the *power distribution*, that must be as similar as possible at each instant of time. Therefore, the batch distribution should avoid high variability of power in the core regions.

This work of thesis is the product of a four months of internship at the division of the *Nuclear Safety, Sustainability, and Security Division* of the Bologna research centre of the *Italian National Agency for the New Technologies, Energy and Sustainable Economic Development* (ENEA). The objective of this internship is to develop an algorithm that allows to find which is the best distribution of fuel assemblies into batches that satisfies the given requirements. In particular, the software developed will be applied to the reference case of the first European Demonstrator Lead-cooled Fast Reactor, ALFRED, whose construction is planned to start after 2030 in the Romanian town of Mioveni.

This thesis is organized as follow. In the first chapter it will be presented an overview of the Generation IV reactors with a focus on the Lead cooled Fast reactors. This chapter will also include a section on the ALFRED reactor to show its main characteristics. The second chapter will explain why a refuelling strategy is necessary and which are the criteria that must be satisfied to obtain the best distribution of fuel assemblies into batches. The next chapter will show the structure of the algorithm that has been developed in the past months, explaining also the opti-

mization algorithm that have been used. Finally, in the last chapter, the results of the application to the ALFRED test case and the proof that the algorithm produce the expected outcomes will be presented. At the end, it will be shown some future development of the algorithm.

Chapter 2

Generation IV Reactors

2.1 Nuclear Reactors Generations

Nuclear fission reactors can be classified based on different parameters, such as the neutrons energies, the purpose of use, the output power, or the coolant. It is also possible to classify them in *Generations*, depending on the used technologies and its safety features. The reactors are usually categorized into four different *Generations* (Figure 2.1):

- *Generation I* refers to the first and early prototypes of civil nuclear reactors, starting from 1942, when the first one was build at University of Chicago. The power of these reactors was very small, below 300 MWe and were mostly *proof-of-concept* reactors. Today, they have been all shut down because most of them lacked of adequate safety systems.

- *Generation II* includes reactors based on the prototype experience. There is the affirmation of technologies such as *Pressurized Water Reactors* (PWR), *CANada Deuterium Uranium reactors* (CANDU), *Boiling Water Reactors* (BWR), *Advanced Gas-cooled Reactors* (AGR) and *Vodo-Vodyanoi Energetichesky Reactors* (VVER). Generation II reactors began operations at the end of the 1960s and are characterized by an increased power output, up to 1000 MWe. These reactors require relatively large electrical grids and produce a certain quantity of nuclear waste that must be disposed in a high-level radioactive waste repository.

- *Generation III* reactors are essentially reactors of Generation II with evolutionary and state-of-the-art improvements. These regard fuel technologies, thermal efficiency and safety features, in particular the usage of passive safety

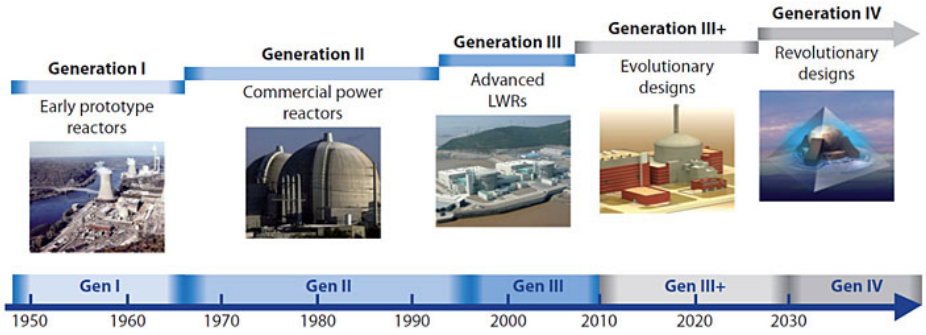

Figure 2.1. Time ranges corresponding to the design and the first deployment of different generations of reactors. [4]

systems, which are triggered by physical phenomena instead of being activated by operators. With respect to Generation II, these reactors have a longer operational life, up to 60 years.

Generation III+ reactors are the evolution and the development of the Generation III ones. The major enhancements regard mostly the safety systems, which now heavily rely on the use of passive safety features, exploiting gravity and natural convection of fluids, to shut down the core. For instance, this type of reactor would have prevented accidents like the one in Fukushima. This kind of reactor is designed to burn more fertile and fissile atoms and therefore a lower, but still relevant, amount of nuclear waste is produced.

Nowadays, the *Generation III+* reactors are the most advanced and commercially available reactors, but we are already studying for the next generation of nuclear reactors.

2.2 Generation IV Reactors Program

In 2000, Argentina, Brazil, Canada, France, Japan, South Korea, South Africa, the UK and the USA got together and founded the *Generation IV International Forum* (GIF). In the following years other countries, that considered the nuclear energy vital for the future, joined this program, forming a group of 13 members. GIF is an international collaboration born to share the knowledge between the members in order to establish the feasibility and the performances of the next generation of nuclear reactors. The GIF has defined eight objectives that a generation IV reactor should satisfy. The objectives can be differentiated into four broad pillars: *Sustainability*, *Safety and reliability*, *Economics* and *Proliferation resistance and*

physical protection[4]:

Sustainability Sustainability is defined by the World Commission on Environment and Development as:

> the ability to satisfy the needs we have today, without compromising the ability for the future generations to meet their own needs [5].

Sustainability requires the conservation of the natural resources and the protection of the environment. The GIF defined the goals of the sustainability, with a focus on waste management and resource utilization. Uranium, that is the raw material for the working of a nuclear reactor, is a limited resource and its demand will grow as well as the electricity demand will do in the next years [6], in order to move away from fossil fuels.

Natural uranium is composed for the 99.3% of ^{238}U and just for the 0.7% of ^{235}U [7], the fissile isotope of uranium required for the fission reaction in existing thermal reactors. To increase the concentration of this isotope, the natural uranium is enriched to a percentage between 3% and 6% (Low Enriched Uranium). In a thermal reactor this kind of fuel is used, but just the fissile uranium is exploited as fuel, while the remaining part of the uranium does not contribute significantly to the production of energy. In the fast reactors, the fast spectrum of neutrons allows certain elements, such as ^{238}U and ^{232}Th, known as *fertile* materials, to efficiently capture neutrons and transmute into *fissile* isotopes (Section 2.3.3), specifically ^{239}Pu and ^{233}U, respectively. This transformation contributes to the overall reduction of nuclear waste through effective management and recycling of fissile materials. A reactor in which the fissionable atoms produced, starting from the fertile ones are more (or at least equal) with respect to the ones burned, is called *breeder* reactor. Furthermore, in both LWRs and lead cooled fast reactor, the neutron capture process results in the formation of the Minor Actinides (MA) in the nuclear waste. Unlike the waste produced by light water reactors (LWRs), which contains long-lived isotopes with half-lives on the order of hundreds of thousands of years and sent directly to the waste disposal, the MAs in lead-cooled fast reactor waste can be included in the reprocessed fuel to be burnt again. This reduces significantly the quantity of the long half-life elements to be sent to the high level site, typically to the range of hundreds of years. This distinction significantly reduces the overall radiotoxicity and decay time of the nuclear waste, making it more manageable. Therefore, developing a reactor that works in the fast spectrum, without the necessity of a moderator that slow down the neutrons up to thermal energy as it happens

in a LWR, is essential in order to reduce the amount and the half time of nuclear waste produced by a nuclear reactor.

Safety and reliability Other important properties of a nuclear reactor of generation IV are safety and reliability. The International Atomic Energy Agency (IAEA) defines the nuclear safety objective as follows:

> The fundamental safety objective is to protect people and the environment from harmful effects of ionizing radiation. [8]

To achieve this objective, nuclear engineering uses the *defense-in-depth* approach, that consists in the use of multiple, independent and redundant barriers between the radioactive source and the external environment. In that way, more of them have to fail for a nuclear accident to cause serious problems to the people and to the environment.

It is typically possible to recognize at least 4 different types of barriers in a nuclear reactor:

- The fuel pellets work as a first barrier;
- The fuel cladding that surrounds the pellets;
- The reactor coolant boundary;
- The containment building.

All the nuclear reactors have also safety systems that are triggered by some particular situations to mitigate or nullify the damages of an accident. It is possible to distinguish two types of safety systems: *active* and *passive* systems. The first ones are triggered by an electrical signal or by an operator, while the seconds are based on physical phenomena, such as gravity or natural convection of the coolant and are triggered spontaneously in case of malfunctioning.

The generation IV nuclear reactors will reinforce the *defense-in-depth* approach, by utilizing inherent safety and passive systems.

Economics The third important aspect of a generation IV reactor is the economics.

Today most of the reactors are owned by government or by regulated private company, while in the future nuclear reactor system should have several options

of ownership, with the possibility to be used also for different purpose beyond electricity production, such as the hydrogen production or district heating.

The economic competitiveness is another economical aspect that must be considered for the success of a nuclear reactor. The life cycle cost advantage must be clear and the financial risk comparable with the other energy sources.

Proliferation resistance and physical protection The last attributes, a generation IV reactor will have, are the added proliferation resistance and physical protection. The definition of *proliferation resistance* of the IAEA is the following:

> The characteristics of a nuclear energy system that impede the diversion of undeclared production of nuclear material or misuse of technology by states in order to acquire nuclear weapons or other nuclear explosive devices. [9]

The technology used for the civil nuclear energy programs partially overlaps with those for the production of fissionable material for nuclear weapons. The primary proliferation risk are not the nuclear power plants, but the enrichment and reprocessing plant.

The reactor of generation IV will take into account these requirements, by making this path very unattractive to the theft of weapon-usable material, and during the design process, it will also be increased the physical protection against acts of terrorism.

In Table 2.1 are reported the eight goals defined by the GIF, divided in the four broad areas.

2.2.1 Technologies of Generation IV reactors

The GIF has originally selected six different promising technologies for the Generation IV program: the *Gas-cooled Fast Reactor* (GFR), the *Lead-cooled Fast Reactor* (LFR), the *Molten Salt Reactor* (MSR), the *Supercritical Water Reactor* (SCWR), the *Sodium-cooled Fast Reactor* (SFR) and the *Very-High Temperature Reactor* (VHTR) [10].

In general, the Generation IV reactors tend to substitute the water with other kind of coolants that allow to work at higher temperatures and therefore higher efficiencies. In addition, the other differences are the neutron spectrum that allows the usage of reprocessed fuel to feed the fast reactor, the possibility to burn also

Sustainability-1	Generation IV nuclear energy systems will provide sustainable energy generation that meets clean air objectives and promotes long-term availability of systems and effective fuel utilization for worldwide energy production.
Sustainability-2	Generation IV nuclear energy systems will minimize and manage their nuclear waste and notably reduce the long-term stewardship burden thereby improving protection for the public health and the environment.
Proliferation Resistance and Physical Protection-1	Generation IV nuclear energy systems will increase the assurance that they are a very unattractive and the least desirable route for diversion or theft of weapons-usable materials and provide increased physical protection against acts of terrorism.
Economics-1	Generation IV nuclear energy systems will have a clear life-cycle cost advantage over other energy sources
Economics-2	Generation IV nuclear energy systems will have a level of financial risks comparable lo other energy projects.
Safety and Reliability-1	Generation IV nuclear energy systems operations will excel in safety and reliability.
Safety and Reliability-2	Generation IV nuclear energy systems will have a very low likelihood and degree of reactor damage.
Safety and Reliability-3	Generation IV nuclear energy systems will eliminate the need for off-site emergency response.

Table 2.1. The eight goals for a Generation IV reactor established by the GIF.

isotopes that do not produce fission in thermal reactors, such as ^{238}U, the closure of the fuel cycle, and the size of the nuclear reactor.

Their main characteristics are summed up in Table2.2.

2.3 Lead Cooled Fast Reactor

With the Sodium Fast Reactor, the Lead Fast Reactor (LFR) is one of the liquid metal cooled reactors in the Generation IV program.

Finding a person or organization that first conceived a LFR can be challenging, because the development happened on parallel research lines on different countries. In any case, there are some clues that suggest that the idea of heavy metal cooled

Technology	Neutron Spectrum	Coolant	Fuel Cycle	T [°C]	Size
GFR	Fast	Helium	Closed	850	Big
LFR	Fast	Lead or Pb-Bi	Closed	480-570	Small Big
MSR	Fast or Thermal	Fluoride Salts	Closed or Open	700-800	Big
SFR	Fast	Sodium	Closed	500-550	Small Big
SCWR	Fast or Thermal	Water	Closed or Open	510-625	Big
VHTR	Thermal	Helium	Open	900-1000	Small

Table 2.2. In this table are reported the main characteristics of the six (seven) technologies selected by the GIF. [10]

reactor was first proposed in the 1950s in the U.S.A. Despite that, about ten years later most of the research groups moved towards the Sodium Fast Reactor. From the 1950s to 1980s, the Soviet Union made the major improvements in the reactor design of lead reactors, in particular for the specific purpose of the submarine propulsion [11].

In more recent times, surely remarkable is the *European Lead-cooled System* (ELSY), co-founded by the *European Atomic Energy Community* (EURATOM) and coordinated by the Italian Ansaldo Nucleare S.p.A.. With this project, Ansaldo aimed at the demonstration that it is possible to design a competitive and safe fast power reactor using simple technical engineered features [12]. At the end of the ELSY project, the LFR development continued with the LEADER project (Lead-cooled European Advanced DEmonstration Reactor), started in April 2010. LEADER had as objectives to solve the issues raised by the previous project and to define the characteristics of the demonstration reactor called ALFRED, that will be presented in Section 2.4.

LFRs use molten lead as coolant in the reactor. Given the good properties of lead, that will be discussed in the Section 2.3.1, it is possible to operate at higher temperatures with respect to the water reactor, increasing the efficiency in the heat exchanger between the primary and secondary circuit and, therefore, the total efficiency of the reactor. Since lead does not act as moderator and neutrons interact via scattering with lead, it allows these reactors to operate in the fast spectrum, enabling the fast fission process and the closure of the fuel cycle, minimizing nuclear waste and optimizing nuclear resource utilization.

2.3.1 Lead Properties

Two different coolants have been studied as candidate for LFR reactors: molten pure lead and a molten lead bismuth eutectic alloy. This choice has been made due to the lead properties [11] that will be hereafter illustrated.

Melting Temperature The melting temperature of pure lead at normal condition is:

$$T_{melt} = (600.6 \pm 0.1)\mathrm{K}$$

and it increases by 0.0792 K per 1 MPa. It is higher than the one of water, so the operating temperature must be higher of T_{melt}. This is not a problem during the operation, but it could become an issue during the refuelling process, because the temperature may decrease, and the lead may solidify. Because of its lower melting temperature, also a lead-bismuth eutectic (LBE) alloy candidate has been studied as coolant.

Boiling Temperature Both lead and LBE have a very high boiling temperatures respectively, just above and below 2000 K. Therefore, it is not necessary to pressurize the core even at high temperature, resulting in a safer reactor with a reduced risk of *loss of coolant* accidents.

Thermal Conductivity The thermal conductivity of molten lead increases linearly with the temperature:

$$\lambda_{\mathrm{Pb}} = 9.2\,\mathrm{W\,m^{-1}\,K^{-1}} + 0.011\,\mathrm{W\,m^{-1}\,K^{-2}} \cdot T[\mathrm{K}]$$

Therefore, since the operational temperature reaches values between 500-600 °C, the thermal conductivity is larger than $17\,\mathrm{W\,m^{-1}\,K^{-1}}$. As reference, here is reported the water thermal conductivity of $0.6\,\mathrm{W\,m^{-1}\,K^{-1}}$.

Neutrons and Gamma Shielding Lead and LBE have both good neutronic properties indeed, they are almost transparent to neutrons that do not lose their energy.

They are also effective in shielding gamma radiation.

Density Lead has a very high density, around $11\,340\,\mathrm{kg\,m^{-3}}$. The load the structure is subject to under a seismic event must be taken into account, and the com-

ponents and the structures must be anchored.

Chemical Properties Lead and LBE are chemically inert. That means that they do not interact readily with water and air, avoiding the ignitions that could happen in sodium fast reactors. The inertness allows the engineers to simplify the reactor design and remove the intermediate circuit, resulting in a lower initial investment. In addition, they show a very good retention capacity of fission products, that drastically reduce the risk of the fission products leakage in the event of an accident.

Corrosion In the usage of lead or LBE there are some negative aspects to take into account. Firstly, there is the corrosion of the steels caused by lead or LBE. This problem can be reduced controlling the quantity of oxygen dissolved in the coolant. The oxygen atoms create an oxide layer on the walls of the surface of the steels, which works as a corrosion barrier. This works fine just for temperatures below 480 °C. For higher temperatures, up to 600 °C, the corrosion resistance of structural materials can be enhanced by a coating.

Polonium Production Another problem in the usage of LBE and, to a much minor degree, lead is the production of polonium: ^{209}Bi can capture a neutron, becoming therefore ^{210}Bi, that can decay β^- to ^{210}Po:

$$^{209}\text{Bi} + n \longrightarrow {}^{210}\text{Bi} \xrightarrow{\beta^-} {}^{210}\text{Po}$$

^{210}Po is a powerful α emitter that make more difficult the refuelling and maintenance because it cannot be ignored during this process.

The ^{210}Po is produced by another mechanism, also employing a pure lead coolant, but the quantity produced is four orders of magnitude smaller.

In conclusion, using lead as coolant results in several benefits, such as an increased reactor efficiency and safety, simplification of the design and therefore lower initial investment.

2.3.2 Fast Neutron Fission

Neutrons are classified depending on their energy in several categories. In ascending order of energy we can find *cold*, *thermal*, *epithermal*, *intermediate*, *fast* and *relativistic*. The *thermal* ones are free neutrons that have an energy corresponding to the most probable speed at room temperature, therefore an energy of about

0.025 eV. The *fast* ones, are instead neutrons with an energy above 1 MeV and up to 20 MeV.

The thermal reactors work thanks to the fission caused by *thermal* neutrons. Indeed, in this range of energy, the fission cross-section of fissile material such us ^{235}U and ^{239}Pu is of the order of 10^3 b (Figure 2.2), therefore the probability that a fissile atom undergoes fission with a *thermal* neutron is very high. After a fission process, the freed neutrons have an energy that can span between 0.1 MeV and 17 MeV[1] [13] and, to maximize the probability of fission reactions, it is necessary to slow them down, by using a *moderator*.

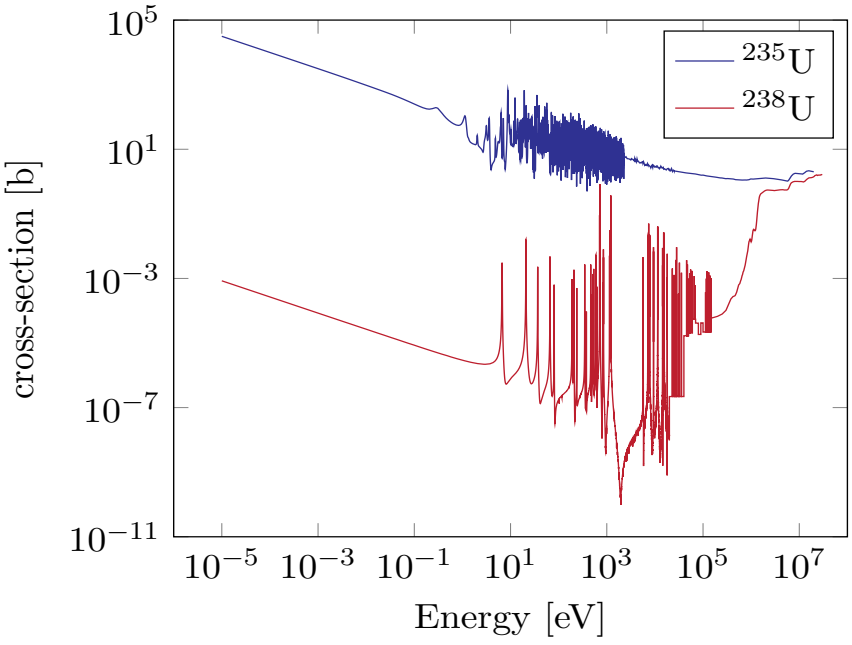

Figure 2.2. Fission cross-section of ^{235}U (in blue) and ^{238}U (in red), in function of the energy. The plot has been produced with data retrieved from [14].

A fast reactor, instead, uses *fast* neutrons to induce fission reactions but, from Figure 2.2 it is possible to see that for high energies the fission cross-section is about three order of magnitude smaller with respect to *thermal* neutrons, therefore a lower number of fissile atoms undergo to a fission reaction. Despite that, also the capture cross-section become smaller and, for this reason, to keep the reactor critical, it is enough to increase the enrichment of the fuel of the fissile atoms, from the few units required for a thermal reactor to the few tens of percentage points required for a fast reactor.

[1] The neutrons have a mean energy of about 2 MeV.

From the same Figure, it is also possible to observe the ^{238}U cross-section. Unlike the fissile materials, this cross-section is very low for low energies and comparable with the one of ^{235}U, for energies corresponding to fast neutrons. That means that, the U238 in a fast reactor contribute partially to the fission process but its major contribution comes from the capture of a neutron that makes it a fissile atom.

2.3.3 Closure of the fuel cycle

In a thermal Light Water Reactor (LWR), the 94% of spent fuel is composed of isotopes of uranium, mostly fertile ^{238}U. The remaining part is fission products (4-5%), plutonium (1%) and minor actinides (0.1%) [15]. With the LWRs it is not possible to burn these isotopes but part of the nuclear waste can be recycled, in particular the ^{238}U and the very small amount of ^{235}U, and ^{239}Pu present (Figure 2.3). These isotopes can be mixed together, with eventually also natural uranium, to form the so-called *Mixed Oxide* (MOX) fuel. The remaining part, that cannot be reprocessed, is sent to a high-level radioactive waste disposal site. With a fast reactor, instead, it is possible to burn a significant portion of the waste components and incorporate them back into a closed fuel cycle for reprocessing. If just uranium and plutonium are recycled, the cycle is called *partially closed*, while if also the minor actinides are recycled, it is *fully closed* (Figure 2.4). Therefore, with a LFR, it is possible to obtain a closed cycle of the fuel and, due to the higher operational temperatures, to get higher efficiencies of the reactors.

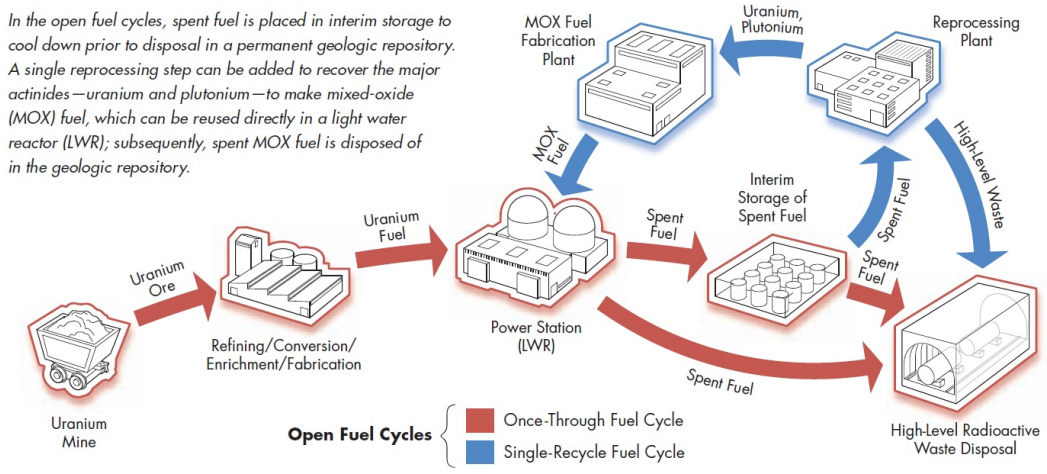

Figure 2.3. Scheme representing the two possible configuration of the open fuel cycle: the red one does not recycle anything, while the blue one, recycle only major actinides such as uranium and plutonium. [15]

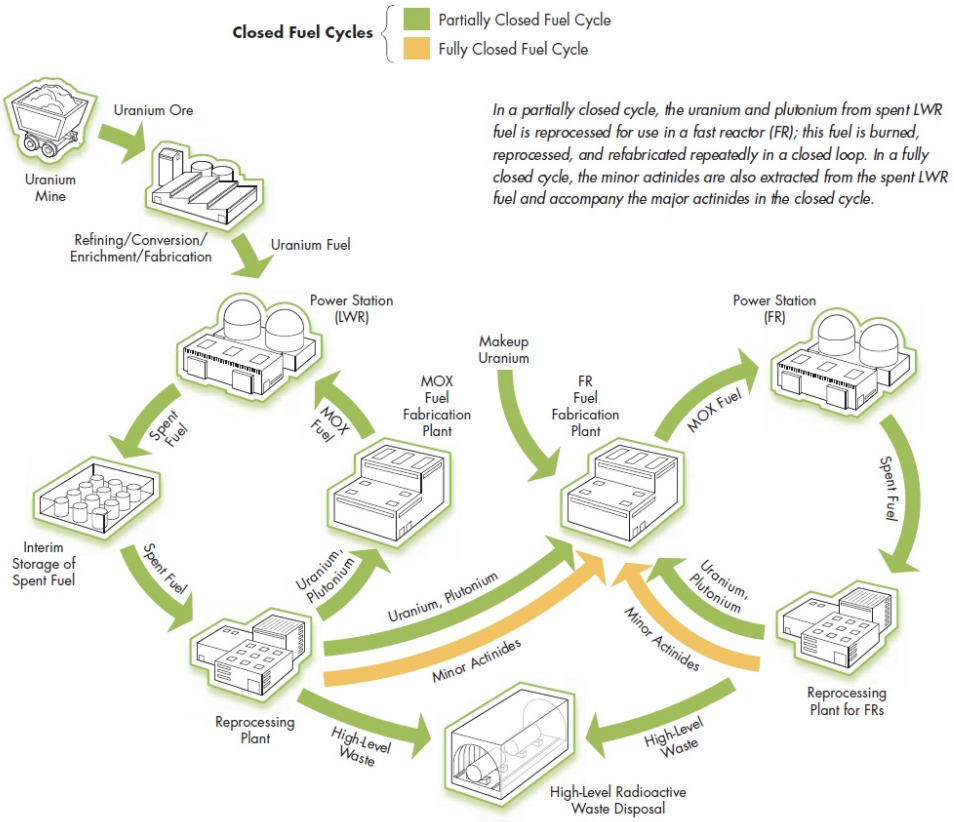

Figure 2.4. Scheme representing the partially closed (green) and fully closed (yellow) fuel cycles. In these two cycles, the spent fuel (uranium and plutonium) is reprocessed many times to produce fuel for fast reactors. In a fully closed process, minor actinides are also reprocessed. [15]

2.4 ALFRED Reactor Core

The *Advanced Lead-cooled Fast Reactor European Demonstrator* (ALFRED) is the demonstrator reactor developed in the frame of the EU FP7 LEADER project. ALFRED is a 300 MWth (125 MWe) pool-type reactor that will be built in the next decade in the Romanian city Mioveni, to demonstrate the viability of the European LFR technology. The coolant is pure lead, and it is characterized by an *inlet temperature* of 400 °C and by an *outlet temperature*[2] of 520 °C.

In this work of thesis, the developed algorithm has been applied to the test case of the ALFRED reactor core. For this reason, in this section will be described only the elements of the core structure that will be of our interest.

The ALFRED core (Figure 2.5) is made of hexagonal sub-assemblies, distin-

[2]Inlet and outlet temperatures refer respectively to the temperature at which lead enters the core and leaves it.

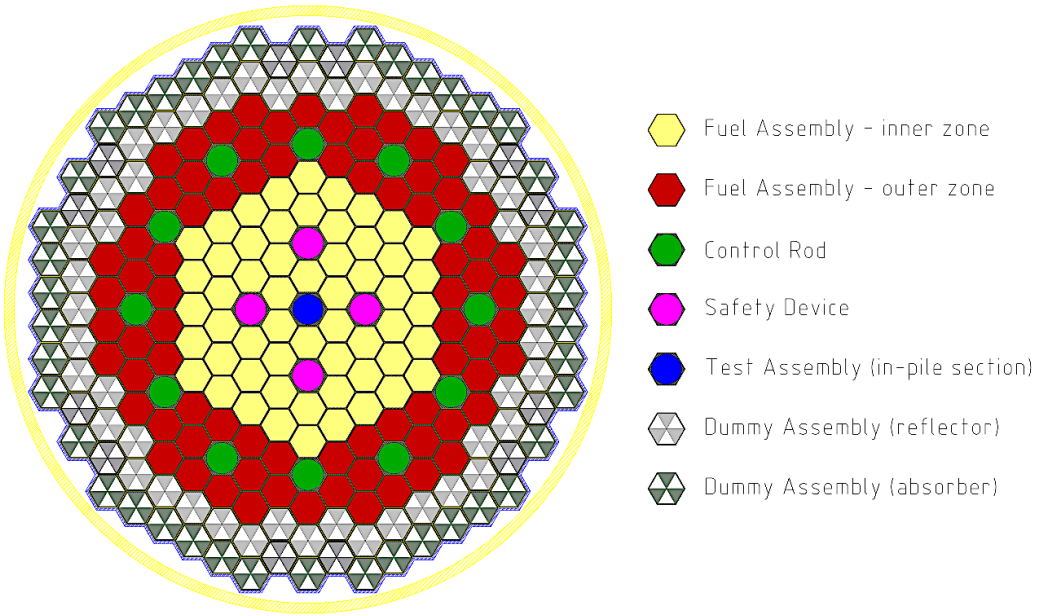

Figure 2.5. ALFRED core map representation. [16]

guished in *Fuel Assemblies* (FA), *Control Rods* (CR), *Safety Rods* (SR), Reflector and Shielding. In addition, the central sub-assembly is dedicated to testing. Each FA has an internal structure: they are formed by 127 pins containing the fuel pellets. The coolant flows between these pins, removing the heat produced during the fission process. The fuel pellets are not located on the whole length of the pins, but just in a region of 81 cm of length, called *active region*. The remaining region is made up of two *plena*: both are filled with gases produced during the fission process, and one also contains a spring that keeps the fuel in the right position.

The FA are pushed down to avoid the floating due to the higher coolant density. In the ALFRED core the FA contains *Mixed Oxide* (MOX) fuel with different enrichment: in the centre of the core 56 FA have an enrichment of 20.5 wt.% in $PuO_{1.97}$, while in the outermost part the remaining 78 FA have an enrichment of 26.2 wt.%, for a total of 134 FA. The reason for using two types of enrichment is to reduce the peak of the power distribution among the core and the consequent inhomogeneous burning of the fuel, that we would have in the case of a single enrichment (Figure 2.6). The introduction of the two enrichment region leads to a decrease of power in the innermost region and an increase in the outer one, since the power output is fixed to 300 MWth.

For the reasons we will see in the next Chapter, it resulted convenient to split the refuelling process in phases, or cycles. Each cycle has a duration of 1 year, and it

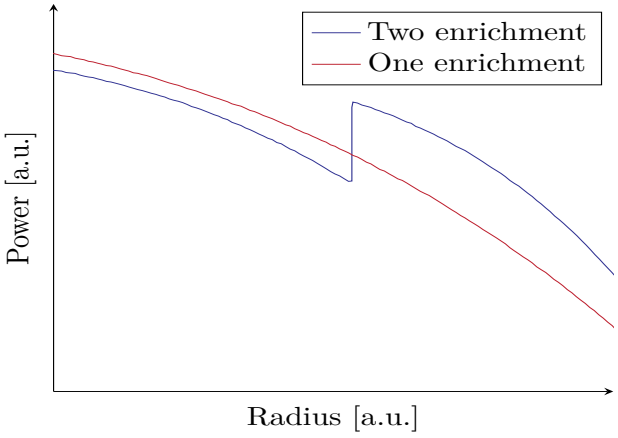

Figure 2.6. Power distribution as a function of the distance from the center of the core in the case of one enrichment (red) and two enrichment (blue). Corresponding to the discontinuity, there is the frontier between the two enrichemnts.

consists in the refuelling of a subset of FA, called *batch*, such that each fuel element stays in the core 5 years. Each cycle defines two instants of time: the *Begin of Cycle* (BoC), when the fresh fuel is positioned into the core and, as a consequence, the control rods are inserted, and *End of Cycle* (EoC), when it is time to remove the depleted fuel and the control rods are extracted.

In the ALFRED core there are 12 CR, situated in the region with the higher enrichment, and are activated during a cycle to regulate the reactivity. When the reactor has to be shut down, in addition to the CR, also the four safety devices in the innermost part are inserted into the core.

Around the outer FA there are 102 *dummy elements*: the first ring of 48 reflector assemblies, that try to reduce the number of neutrons escaping from the core and 54 shielding elements, that are in charge of reducing the amount of radiation that escape from the core.

Chapter 3

Refuelling of nuclear reactors: engineering problems and numerical solutions

3.1 Division of the fuel assemblies into batches

In the previous Chapter, it was mentioned that a nuclear reactor needs that the refuelling of the fuel assemblies happens in several phases and not in just one step. The reason is that, if all the fuel assemblies in the core are substituted with fresh fuel, several issues could arise (as discussed in the following). For this reason, it is preferable to split the refuelling process into cycles that are as similar as possible between them. In that way, in each cycle, just the elements belonging to a specific *batch* are refuelled.

Technically, it is possible to operate a reactor with all the fuel assemblies belonging to the same *batch*; however, due to some design aspects, operation in this regime is inconvenient.

In this Section we will examine the issues that can occur and the main objectives to be satisfied to optimize the reactor.

3.1.1 Reactivity

All the existing commercial nuclear reactors work at the *critical* condition. Theoretically, this means that the reactivity ρ should be 0 and the neutron multiplication factor should be $k_{eff} = 1$ at each instant of time.

The reactivity of the system tends to decrease as the fuel starts to burn. Indeed,

due to the fission reactions, the number of fissile atoms, and therefore the *macroscopic fission cross-section*, starts to decrease, and the *absorption cross-section* starts to increase due to the increase of the fission product. Let us consider for the moment the case in which all the fuel assemblies belong to the same batch. At BoC, since it is necessary an excess of reactivity to compensate the burning of the fuel, the balance between the production and the loss of neutrons is tipped towards the production. Thus, the control rods are fully inserted in the *active region* to decrease the reactivity that otherwise would be higher than zero, leading to a *supercritical* system. When the fuel starts to burn, the decreasing of the reactivity results in a *subcritical* reactor. To compensate this effect, as the fuel burn, the control rods are slowly extracted up to the EoC, when the rod movement alone cannot compensate the effect anymore. This is reflected in a system whose reactivity is almost constant and equals zero along the cycle. Theoretically, it is possible to build such a system, but the problems arise in the design of the control system. To deal with the high reactivity present at BoC, it would be necessary a high number of control rods, comparable with the number of the fuel assemblies. This would result in a more complex system, i.e. one that is larger because it has to contain more assemblies, heavier because, being larger, it has to contain more coolant, and more expensive from an economic point of view. In addition, also the surrounding building must be reinforced because it has to resist to heavier loads in case of earthquakes due to the increased reactor vessel weight.

Instead, in the case of more batches, the control rods have to deal with a smaller quantity of reactivity with respect to the case of one batch. Indeed, at BoC, the excess of reactivity necessary to operate the reactor for a smaller amount of time is smaller. This allows to make a smaller and simpler control system.

In order to optimize the design of the reactivity control system, the best solution is to split in equal parts the excess of reactivity between the cycles. To obtain exactly the same amount of reactivity between the cycles, it is almost impossible. Thus, the system has to be designed in function of the worst possible case (i.e., the case with maximum reactivity and inhomogeneous power distribution) it has to deal. Considering that with a refuelling strategy structured in batches, if the reactivity or power distribution are very good in one cycle, in one of the next ones the situation could be worse, the optimal solution is to make all the cycles as equal as possible in terms of reactivity and power distribution. The reactivity constancy has also a secondary benefit in the refuelling scheduling of the reactor; indeed, if this condition is satisfied, the refuelling happens at regular intervals of time.

3.1.2 Power distribution

In a nuclear reactor, the energy released by fission reactions is transformed into heat, that is removed from the core by the coolant. The power produced in a certain region of the core is proportional to the number of fission reaction that occurs in that region, therefore the amount of power produced in different regions of the core could be different. For this reason, we talk about the power distribution in the reactor core. After the design process of a reactor, the power output and the reactivity are fixed. If all the fuel assemblies contain fresh fuel, then the power distribution, and therefore the temperature distribution, is peaked in the center of the core, while the power produced is lower at the boundary (the distribution is governed by the transport equation, as we will see in Section 3.2.3).

For each component of the core, the limit temperature beyond which the reliability of the component is not ensured anymore, is fixed. In particular, we have to avoid the loss of the radioactivity confinement capacity of the components. This is valid for all the parts of the core, such as the fuel pellets and their cladding. Indeed, for temperatures above 600 °C, lead starts to corrode the cladding. For this reason, it is essential that the lead temperature stays well below this limit temperature in order to ensure the operation of the protective barrier. This can be achieved through a uniform temperature and power distribution. Due to the reasons we have written in the previous Section, it is necessary to introduce the *batches*, even though their introduction worsen the power distribution with respect to the one batch case, for which the enrichment zoning is typically optimized. The distribution of the fuel assemblies into *batches* must therefore limit the penalty on the power and temperature distributions peaks.

The increase of lead temperature could happen locally, therefore it is necessary to avoid clusters of power at each instant of time. This can be achieved by removing or limiting clusters of elements belonging to the same batch, and distributing as homogeneously as possible the batches in the core.

For these reason, it is fundamental to have a power distribution as uniform as possible in the cycle and between the cycles.

3.2 Neutrons Transport Equation

In the following sections, we will see the theory that allowed to model, in a mathematical formulation, the requirements above described. We will start from the neutron transport equation, that describes the motion of the neutrons, to get to

the description of the adjoint transport equation and the importance function, that will be exploited in the model of the requirements.

3.2.1 Assumptions

In the neutron transport theory, some assumptions are usually made to simplify the development of the theory.

The neutron transport theory is based on Boltzmann's equation for neutrons, that has a statistical nature; therefore, also the neutron transport equation is valid just for a statistically relevant number of neutrons. It is usually made the assumption that the neutron is a point-like particle, meaning that we can neglect the neutron-neutron interactions. In facts, for a neutron with an energy of 0.01 eV, the corresponding De Broglie wavelength is significantly smaller than the distances between atoms in a solid and much smaller than both macroscopic dimensions and mean free paths. Consequently, it is reasonable to consider the position of a neutron as a precisely determinable quantity. Indeed, it is possible to determine the position and velocity of a neutron with sufficient precision without violating the Heisenberg's uncertainty principle [17].

In a nuclear reactor, the neutrons produced during the fission process have a fast spectrum. Thus, in a fast reactor, we can assume that of the few thermal neutrons in the reactor, there are basically no neutrons with an energy below 0.01 eV. Therefore, it is possible to avoid the quantum and relativistic description of the neutrons.

3.2.2 Definitions

The *neutron angular density* $N(\mathbf{r}, \mathbf{\Omega}, E, t)$ is defined as the expected number of neutrons in the position $\mathbf{r}$, with a direction $\mathbf{\Omega}$, an energy E, at time t, per unit of volume, solid angle and energy. Therefore, to get the *actual number* of neutrons in a volume $\mathrm{d}V$ about $\mathbf{r}$, with a direction $\mathbf{\Omega}$ around a solid angle $\mathrm{d}\mathbf{\Omega}$ with an energy between E and $E + \mathrm{d}E$, we have to multiply the *neutron angular density* for the infinitesimals:

$$N(\mathbf{r}, \mathbf{\Omega}, E, t)\ \mathrm{d}V\ \mathrm{d}\mathbf{\Omega}\ \mathrm{d}E$$

The integral of *neutron angular density* around all the direction gives us the *neutron density*, n:

$$n(\mathbf{r}, E, t) := \int_{4\pi} N(\mathbf{r}, \mathbf{\Omega}, E, t)\ \mathrm{d}\mathbf{\Omega}$$

From the *neutron angular density*, it is possible to define the *angular neutron*

flux, or *angular flux*, as:

$$\Phi(\mathbf{r}, \mathbf{\Omega}, E, t) := v(E)N(\mathbf{r}, \mathbf{\Omega}, E, t)$$

where $v(E)$ is the magnitude of the velocity of a neutron.

By integration of the neutron angular density over all the directions we obtain the *scalar neutron flux*:

$$\phi(\mathbf{r}, E, t) := \int_{4\pi} v(E)N(\mathbf{r}, \mathbf{\Omega}, E, t)\ \mathrm{d}\mathbf{\Omega} = v(E)n(\mathbf{r}, E, t)$$

The *scalar flux* has the dimension of $[L^{-2}][T^{-1}][E^{-1}]$, therefore it indicates the number of neutrons per unit of area, unit of energy and unit of time.

3.2.3 The equation

The neutron transport equation describes the spatial, energy and time distribution of the neutron angular flux. In this work of thesis, we will give just the expression of the neutron transport equation, without reporting all the passages necessary to obtain the equations. All the steps can be found in [17].

The time-dependent neutron transport equation can be written as follows:

$$\begin{aligned}\left(\frac{1}{v(E)}\frac{\partial}{\partial t} + \ \mathbf{\Omega}\cdot\nabla + \Sigma_t(\mathbf{r},\ E)\right)\Phi(\mathbf{r}, \mathbf{\Omega}, E, t) = \\ = \int_{4\pi}\int_0^\infty \Sigma_s(E' \to E,\ \mathbf{\Omega}' \to \mathbf{\Omega},\ \mathbf{r})\Phi(\mathbf{r}, \mathbf{\Omega}', E', t)\mathrm{d}E'\ \mathrm{d}\mathbf{\Omega}' + \\ + \frac{\chi(E)}{4\pi}\int_0^\infty \nu\Sigma_f(\mathbf{r}, E')\phi(\mathbf{r}, E', t)\mathrm{d}E' + S(\mathbf{r}, \mathbf{\Omega}, E, t)\end{aligned} \tag{3.1}$$

where $\Sigma_t(\mathbf{r},\ E)$ is the *total* macroscopic cross-section, $\Sigma_s(E' \to E,\ \mathbf{\Omega}' \to \mathbf{\Omega},\ \mathbf{r})$ is the *scattering* macroscopic cross-section, $\chi(E)$ is the energy distribution of outgoing neutrons after a fission reaction, $\nu\Sigma_f(\mathbf{r}, E')$ is the *fission* cross-section multiplied by the average number of neutrons emitted per fission, caused by a neutron with energy E', and, finally, $S(\mathbf{r}, \mathbf{\Omega}, E, t)$ represent other sources of neutrons.

In practice, the equation is a balance between the terms that introduce and remove neutrons from our phase space volume of interest.

The first term on the *left-hand side* (LHS) represents the variation in time of the number of neutrons. The second term on the LHS, called the *streaming* term, describes the movement of neutrons that enter and leave the volume of interest. The third term on the LHS takes into account the probability of interaction of the

neutrons with the medium.The first term on the *right-hand side* (RHS) represents the scattering of neutrons from a generic direction $\mathbf{\Omega}'$ to the direction $\mathbf{\Omega}$ into our volume of interest and from an energy E' to an energy E. The second term on the RHS represent instead the production of neutrons through the fission process. Finally, the last term on the RHS represent a generic neutron source.

For simplicity, it will be considered the stationary neutron transport equation, without the time dependence. In that case, the Equation 3.1 can be written as:

$$\begin{aligned}(\mathbf{\Omega}\cdot\nabla+\ \Sigma_t(\mathbf{r},\ E))\,\Phi(\mathbf{r},\mathbf{\Omega},E) = \\ = \int_{4\pi}\int_0^\infty \Sigma_s(E'\to E,\ \mathbf{\Omega}'\to\mathbf{\Omega},\ \mathbf{r})\Phi(\mathbf{r},\mathbf{\Omega}',E')\ \mathrm{d}E'\mathrm{d}\mathbf{\Omega}'+ \\ + \frac{\chi(E)}{4\pi}\int_0^\infty \nu\Sigma_f(\mathbf{r},E')\phi(\mathbf{r},E)\ \mathrm{d}E' + S(\mathbf{r},\mathbf{\Omega},E)\end{aligned} \tag{3.2}$$

The Equation 3.2 can also be written through the use of operators. If we define the *leakage operator* A as:

$$A := -\mathbf{\Omega}\cdot\nabla - \Sigma_t(\mathbf{r},\ E) + \int_{4\pi}\int_0^\infty\ \Sigma_s(E'\to E,\ \mathbf{\Omega}'\to\mathbf{\Omega},\ \mathbf{r})\ \mathrm{d}E'\mathrm{d}\mathbf{\Omega}' \tag{3.3}$$

and the *fission operator* F as:

$$F := -\chi(E)\int_{4\pi}\int_0^\infty \nu\Sigma_f(\mathbf{r},E')\mathrm{d}E'\mathrm{d}\mathbf{\Omega}' \tag{3.4}$$

it is possible to re-write the transport equation as:

$$A\Phi(\mathbf{r},\ \mathbf{\Omega},\ E) - F\Phi(\mathbf{r},\ \mathbf{\Omega},\ E) + S(\mathbf{r},\ \mathbf{\Omega},\ E) = 0$$

The operator A includes all the phenomena that reduce the number of neutrons in the system, while F and S are the responsible for the increase of their number.

When there is no source term in the system, the banal solution is the zero function; however, if we introduce an eigenvalue we can find non-trivial solutions. There are several possibilities on which eigenvalue to introduce, but the most common choice is to use the eigenvalue $1/k$, where k is the so-called *neutron multiplication factor*, that multiplies the fission term:

$$T\Phi(\mathbf{r},\ \mathbf{\Omega},\ E) := A\Phi(\mathbf{r},\ \mathbf{\Omega},\ E) - \frac{F}{k}\Phi(\mathbf{r},\ \mathbf{\Omega},\ E) = 0 \tag{3.5}$$

If $k = 1$ the balance between the production of neutrons by fission and the loss of neutrons is perfectly balanced and therefore, the number of neutrons stays constant.

In the case $k > 1$, it means that the fission must be reduced to allow a steady state solution to exist and, thus, the number of neutron is increasing. Finally, if $k < 1$, we have that to balance the equation it is necessary to increase the fission and therefore it means that the number of neutrons in the system is decreasing.

For simplicity, we will call T, the total transport operator, as in Equation 3.5.

3.3 Adjoint Transport Equation

In the next passages it will be defined the *adjoint* of an operator and the resulting *adjoint transport equation*, that will lead to the definition of the *neutron importance*.

3.3.1 Inner product

Before defining the adjoint of an operator, it is important to define the inner product between two functions. Given two functions $\varphi(\boldsymbol{\xi})$ and $\psi(\boldsymbol{\xi})$ of the same variables set $\boldsymbol{\xi}$, the inner product $\langle \varphi(\boldsymbol{\xi}) \mid \psi(\boldsymbol{\xi}) \rangle$ can be defined as:

$$\langle \varphi(\boldsymbol{\xi}) \mid \psi(\boldsymbol{\xi}) \rangle := \int \varphi(\boldsymbol{\xi}) \psi(\boldsymbol{\xi}) d\boldsymbol{\xi}$$

where the integral is extended all over the full range of the variables' domain. The equation above defines an inner product, which has all the typical properties of an inner product. For all ϕ, ζ, ψ functions of the variables $\boldsymbol{\xi}$ and for all $\lambda, \mu \in \mathbb{R}$ the inner product is:

- **Linear**: $\langle \lambda\phi + \mu\zeta \mid \psi \rangle = \lambda \langle \phi \mid \psi \rangle + \mu \langle \zeta \mid \psi \rangle$
- **Symmetric**: $\langle \phi \mid \psi \rangle = \langle \psi \mid \phi \rangle$
- **Positive Semi-Definite**: $\langle \phi \mid \phi \rangle \geq 0$ and $\langle \phi \mid \phi \rangle = 0 \iff \phi = 0$

With this definition, given an operator O, we define its *adjoint operator* $O^\dagger$, such that:

$$\langle \varphi(\boldsymbol{\xi}) \mid O\psi(\boldsymbol{\xi}) \rangle = \left\langle O^\dagger \varphi(\boldsymbol{\xi}) \,\middle|\, \psi(\boldsymbol{\xi}) \right\rangle \tag{3.6}$$

3.3.2 The Equation

Following the definition of the adjoint of an operator in the previous subsection, we define the *adjoint leakage operator*, $A^\dagger$, as follows:

$$\left\langle A\Phi \,\middle|\, \Phi^\dagger \right\rangle = \left\langle \Phi \,\middle|\, A^\dagger \Phi^\dagger \right\rangle \tag{3.7}$$

where $\Phi^\dagger$ is the *adjoint function*. Both Φ and $\Phi^\dagger$ are assumed to be continuous functions and have to satisfy some boundary conditions. It is important to remember that in this case the integral of the inner product is over the energy, the volume, and the direction.

By explicitly writing the inner products of the Equation 3.7 and using the expression of the *direct leakage operator*, we can get the expression of the *adjoint leakage operator* that can be written as:

$$A^\dagger = +\mathbf{\Omega}\cdot\nabla - \Sigma_t(\mathbf{r},\ E) + \int_{4\pi}\int_0^\infty \Sigma_s(E\to E',\ \mathbf{\Omega}\to\mathbf{\Omega}',\ \mathbf{r})\ \mathrm{d}E'\mathrm{d}\mathbf{\Omega}' \tag{3.8}$$

Compared to the expression of the direct leakage operator of Equation 3.3, we notice the difference in the sign of the *streaming* term and the reverse order of the variables in the scattering cross-section. Indeed, now we consider the neutrons scattered towards any direction $\mathbf{\Omega}'$ of the space and with any value of energy E'.

In the same way, we can compute also the *adjoint fission operator*, that becomes:

$$F^\dagger = -\nu\Sigma_f(E)\int_{4\pi}\int_0^\infty \chi(\mathbf{r},E')\mathrm{d}E'\ \mathrm{d}\mathbf{\Omega}' \tag{3.9}$$

Once that the adjoint source has been fixed (Section 3.4), it is possible to write the *adjoint transport equation*:

$$A^\dagger\Phi^\dagger(\mathbf{r},\ \mathbf{\Omega},\ E) - F^\dagger\Phi^\dagger(\mathbf{r},\ \mathbf{\Omega},\ E) + S^\dagger(\mathbf{r},\ \mathbf{\Omega},\ E) = 0 \tag{3.10}$$

3.4 Adjoint Function and Importance

In the previous section, we have introduced the *adjoint function*. It is important to understand that the *adjoint function* assumes a different meaning according to the adjoint source, $S^\dagger$. We will now find out which is the physical meaning of $\Phi^\dagger$ that satisfies the Equation 3.10. Let us consider the transport equation and its adjoint, for a subcritical system, therefore with a source term $S(\mathbf{r},\mathbf{\Omega},E)$:

$$A\Phi - F\Phi = -S \tag{3.11a}$$

$$A^\dagger\Phi^\dagger - F^\dagger\Phi^\dagger = -S^\dagger \tag{3.11b}$$

with the boundaries condition that the entering angular flux is 0 at the boundary of the considered region, and its exiting adjoint is 0 at the boundaries[1]. The physical

[1]These boundaries are necessary to obtain the expression of the adjoint operators as have been presented

significance of the adjoint function, can be understood by arbitrarily defining the adjoint source term as the response [17], proportional to the macroscopic cross-section, of a neutron detector positioned in $\mathbf{r}$ and energy E. Therefore,

$$S^\dagger(\mathbf{r}, \mathbf{\Omega}, E) = \Sigma(\mathbf{r}, E)$$

By performing the inner product between Equation 3.11a and $\Phi^\dagger$, and between Equation 3.11b and Φ, by adding the two equations we get the following relation:

$$\left\langle A\Phi \,\middle|\, \Phi^\dagger \right\rangle - \left\langle F\Phi \,\middle|\, \Phi^\dagger \right\rangle + \left\langle S \,\middle|\, \Phi^\dagger \right\rangle = \left\langle \Phi \,\middle|\, A^\dagger\Phi^\dagger \right\rangle - \left\langle \Phi \,\middle|\, F^\dagger\Phi^\dagger \right\rangle + \langle \Phi \mid \Sigma \rangle$$

Using the definition in Equation 3.6, the terms with A and F vanish and, integrating, we obtain:

$$\iiint S(\mathbf{r}, \mathbf{\Omega}, E)\Phi^\dagger(\mathbf{r}, \mathbf{\Omega}, E)\ \mathrm{d}V\mathrm{d}\mathbf{\Omega}\ \mathrm{d}E = \iiint \Sigma(\mathbf{r}, E)\Phi(\mathbf{r}, \mathbf{\Omega}, E)\ \mathrm{d}V\mathrm{d}\mathbf{\Omega}\ \mathrm{d}E$$

Since the source S is arbitrary [17], it can be defined as $S(\mathbf{r}, \mathbf{\Omega}, E) = \delta(\mathbf{r}_0, \mathbf{\Omega}_0, E_0)$, therefore:

$$\Phi^\dagger(\mathbf{r}_0, \mathbf{\Omega}_0, E_0) = \iiint \Sigma(\mathbf{r}, E)\Phi(\mathbf{r}, \mathbf{\Omega}, E)\ \mathrm{d}V\mathrm{d}\mathbf{\Omega}\ \mathrm{d}E$$

From this expression we understand that the *adjoint function* or *importance* of a neutron positioned in $\mathbf{r}_0$, with a direction $\mathbf{\Omega}_0$ and with an energy E_0 is a measure of how much it contributes to the response of the detector previously positioned. That gives a physical meaning to the boundary condition: the importance of a neutron in the proximity of the boundaries of the space-region of interest, with an exiting direction, is zero. Indeed, it will not contribute in any case to the detector response.

It is important to remember that the choice of the detector is arbitrary: changing the detector, leads to different equations and different adjoint function. If the adjoint source is defined as the fission event in the system then $\Phi^\dagger$ is named *importance* or *adjoint flux*, while if we are interested in other parameter, such as the power production, the adjoint is called *generalized importance*.

3.5 Perturbation theory

Let us suppose to have a system subject to a small change (or *perturbation*), that is reflected in a change in the reactivity or in the power distribution. Instead of repeating a new exact simulation of the entire system, that takes hours of computation, it is possible to predict the response of the system to that change with

the perturbation theory, that employs just few seconds. The perturbation can be, for example, a change in the *macroscopic cross-section* $\Sigma = \sigma \cdot \mathcal{N}$, where σ is the *microscopic cross-section* and $\mathcal{N}$ is the number density of the atoms. It is possible to determine the effects of the perturbation with different level of approximation. In this work of thesis, it will be considered just the first order approximation, because it provides good results without committing big errors. Therefore, all the terms in which the perturbation is squared, will be neglected. To predict the effect of the perturbations, this theory makes use of the *adjoint function* that we have seen in the previous Section.

Let us consider a steady-state system, without the source of neutrons. In such a case, it is necessary to introduce the factor k, in order to balance the equation between the loss and the production. The transport equation for the eigenvalue $1/k$, for the unperturbed system is

$$\begin{aligned}\boldsymbol{\Omega} \cdot \nabla\Phi(\mathbf{r}, \boldsymbol{\Omega}, E) + \Sigma_t(\mathbf{r}, E)\Phi(\mathbf{r}, \boldsymbol{\Omega}, E) = \\ = \iint \Sigma_s(E' \to E,\ \boldsymbol{\Omega}' \to \boldsymbol{\Omega},\ \mathbf{r})\Phi(\mathbf{r}, \boldsymbol{\Omega}', E')\ \mathrm{d}\boldsymbol{\Omega}'\ \mathrm{d}E' + \\ + \frac{\chi(E)}{k} \iint\ \frac{1}{4\pi}\nu\Sigma_f(\mathbf{r}, E')\Phi(\mathbf{r}, \boldsymbol{\Omega}', E')\ \mathrm{d}\boldsymbol{\Omega}'\ \mathrm{d}E'\end{aligned} \tag{3.12}$$

while its adjoint equation, for the eigenvalue $1/k^\dagger$, is:

$$\begin{aligned}-\boldsymbol{\Omega} \cdot \nabla\Phi^\dagger(\mathbf{r}, \boldsymbol{\Omega}, E) + \Sigma_t(\mathbf{r}, E)\Phi^\dagger(\mathbf{r}, \boldsymbol{\Omega}, E) = \\ = \iint \Sigma_s(E \to E',\ \boldsymbol{\Omega} \to \boldsymbol{\Omega}',\ \mathbf{r})\Phi^\dagger(\mathbf{r}, \boldsymbol{\Omega}', E')\ \mathrm{d}\boldsymbol{\Omega}'\ \mathrm{d}E' + \\ + \frac{\nu\Sigma_f(\mathbf{r}, E)}{k^\dagger} \iint\ \frac{1}{4\pi}\chi(E')\Phi^\dagger(\mathbf{r}, \boldsymbol{\Omega}', E')\ \mathrm{d}\boldsymbol{\Omega}'\ \mathrm{d}E'\end{aligned} \tag{3.13}$$

For the fundamental (i.e. the largest) eigenvalue, it can be shown that $k = k^\dagger$ [17]. Considering the perturbations $\tilde{\Sigma}_t := \Sigma_t + \delta\Sigma_t$, $\tilde{\Sigma}_s := \Sigma_s + \delta\Sigma_s$, $\tilde{\nu}\tilde{\Sigma}_f := \nu\Sigma_f + \delta\nu\Sigma_f$, $\tilde{\Phi} := \Phi + \delta\Phi$, and perturbed eigenvalue $\tilde{k}$, we can get the transport equation for the perturbed system:

$$\begin{aligned}\boldsymbol{\Omega} \cdot \nabla\tilde{\Phi}(\mathbf{r}, \boldsymbol{\Omega}, E) + \tilde{\Sigma}_t(\mathbf{r}, E)\tilde{\Phi}(\mathbf{r}, \boldsymbol{\Omega}, E) = \\ = \iint \tilde{\Sigma}_s(E' \to E,\ \boldsymbol{\Omega}' \to \boldsymbol{\Omega},\ \mathbf{r})\tilde{\Phi}(\mathbf{r}, \boldsymbol{\Omega}', E')\ \mathrm{d}\boldsymbol{\Omega}'\ \mathrm{d}E' + \\ + \frac{\chi(E)}{\tilde{k}} \iint\ \frac{1}{4\pi}\tilde{\nu}\tilde{\Sigma}_f(\mathbf{r}, E')\tilde{\Phi}(\mathbf{r}, \boldsymbol{\Omega}', E')\ \mathrm{d}\boldsymbol{\Omega}'\ \mathrm{d}E'\end{aligned} \tag{3.14}$$

Multiplying 3.13 by $\tilde{\Phi}$ and 3.14 by $\Phi^\dagger$, subtracting one by the other, and integrating

we obtain:

$$\begin{aligned}
\delta\Sigma_t \left\langle \tilde{\Phi}(\mathbf{r},\mathbf{\Omega},E) \,\middle|\, \Phi^\dagger(\mathbf{r},\mathbf{\Omega},E) \right\rangle = \\
= \iint \left\langle \tilde{\Phi}(\mathbf{r},\mathbf{\Omega}',E') \,\middle|\, \delta\Sigma_s(\mathbf{r},\mathbf{\Omega}'\to\mathbf{\Omega},E'\to E)\Phi^\dagger(\mathbf{r},\mathbf{\Omega},E) \right\rangle \mathrm{d}\mathbf{\Omega}'\ \mathrm{d}E' + \\
+ \frac{1}{\tilde{k}}\frac{1}{4\pi} \iint \left\langle \tilde{\Phi}(\mathbf{r},\mathbf{\Omega}',E') \,\middle|\, \nu\tilde{\Sigma}_f(\mathbf{r},E')\chi(E)\Phi^\dagger(\mathbf{r},\mathbf{\Omega},E) \right\rangle \mathrm{d}\mathbf{\Omega}'\ \mathrm{d}E' + \\
- \frac{1}{k^\dagger}\frac{1}{4\pi} \iint \left\langle \tilde{\Phi}(\mathbf{r},\mathbf{\Omega}',E') \,\middle|\, \nu\Sigma_f(\mathbf{r},E)\chi(E')\Phi^\dagger(\mathbf{r},\mathbf{\Omega},E) \right\rangle \mathrm{d}\mathbf{\Omega}'\ \mathrm{d}E'
\end{aligned} \tag{3.15}$$

By exchanging the variables name (E with E') in the last term in the RHS, and using the relation

$$\frac{1}{\tilde{k}} = \frac{1}{k^\dagger} - \frac{1}{k} + \frac{1}{k} = -\frac{\delta k}{k\tilde{k}} + \frac{1}{k}$$

and neglecting the second order terms, we obtain:

$$\begin{aligned}
\frac{1}{4\pi}\frac{\delta k}{k\tilde{k}} \iint \left\langle \Phi(\mathbf{r},\mathbf{\Omega}',E') \,\middle|\, \nu\Sigma_f(\mathbf{r},E')\chi(E)\Phi^\dagger(\mathbf{r},\mathbf{\Omega},E) \right\rangle \mathrm{d}\mathbf{\Omega}'\ \mathrm{d}E' = \\
= \iint \left\langle \Phi(\mathbf{r},\mathbf{\Omega}',E') \,\middle|\, \delta\Sigma_s(\mathbf{r},\mathbf{\Omega}'\to\mathbf{\Omega},E'\to E)\Phi^\dagger(\mathbf{r},\mathbf{\Omega},E) \right\rangle \mathrm{d}\mathbf{\Omega}'\ \mathrm{d}E' + \\
+ \frac{1}{4\pi}\frac{1}{k} \iint \left\langle \Phi(\mathbf{r},\mathbf{\Omega}',E') \,\middle|\, \delta\nu\Sigma_f(\mathbf{r},E')\chi(E)\Phi^\dagger(\mathbf{r},\mathbf{\Omega},E) \right\rangle \mathrm{d}\mathbf{\Omega}'\ \mathrm{d}E' + \\
- \left\langle \Phi(\mathbf{r},\mathbf{\Omega},E') \,\middle|\, \delta\Sigma_t(\mathbf{r},E)\Phi^\dagger(\mathbf{r},\mathbf{\Omega},E) \right\rangle
\end{aligned} \tag{3.16}$$

This equation can be simplified with the usage of operators previously defined (Equation 3.3 and Equation 3.4), reminding that the scattering part is included in the leakage term. Starting respectively from the terms on the RHS of the previous equation, we can write the change of the reactivity with respect to the initial configuration, taking into account that for small perturbation $\tilde{k} \simeq k$, as

$$\delta\rho = \frac{\delta k}{k^2} = \frac{\left\langle \Phi^\dagger \middle|\, \frac{\delta F}{k}\Phi \right\rangle - \left\langle \Phi^\dagger \middle|\, \delta A\Phi \right\rangle}{\langle \Phi^\dagger |\ F\Phi \rangle} \tag{3.17}$$

where δF and δA correspond respectively to Equations 3.4 and 3.3 in which the cross-sections are substituted by their respectively variations. It is crucial to observe that in the Equation 3.17, neither $\tilde{\Phi}$ nor $\tilde{\Phi}^\dagger$ appear, but just the variation of the cross-sections and Φ and $\Phi^\dagger$. Therefore, with just one computation of the flux and the adjoint flux, we can directly link the cross-section variation with the corresponding reactivity change, without repeating the time-consuming computations.

The theory seen up to now is called *standard perturbation theory.*

3.5.1 Generalized Perturbation Theory

If we want to investigate the effects on parameters other than k, we employ a *generalized perturbation theory* [18]. In particular, given a perturbation on the macroscopic cross-section, and a homogeneous functional of degree zero in the direct and adjoint flux, $f(\Sigma, \Phi, \Phi^\dagger)$, that satisfies the relation $f(\Sigma, \lambda\Phi, \mu\Phi^\dagger) = f(\Sigma, \Phi, \Phi^\dagger)$ for any scalars λ and μ, it is possible to determine the effects df.

Let us consider a critical system, in which the constraints on the flux and the adjoint flux are:

$$\left(A - \frac{F}{k}\right)\Phi = 0 \quad \text{and} \quad \left(A^\dagger - \frac{F^\dagger}{k}\right)\Phi^\dagger = 0 \tag{3.18}$$

It is important to remind that in the expression of A it is present also the scattering term. In order to find the expression of the δf, we introduce two fixed Lagrange multipliers Ψ and $\Psi^\dagger$ and we consider the functional L, defined as

$$L := f(\Sigma, \Phi, \Phi^\dagger) - \left\langle \Psi^\dagger \,\middle|\, \left(A - \frac{F}{k}\right)\Phi \right\rangle - \left\langle \Psi \,\middle|\, \left(A^\dagger - \frac{F^\dagger}{k}\right)\Phi^\dagger \right\rangle$$

then we compute its variation:

$$\begin{aligned} dL = &\left\langle \frac{\partial f}{\partial \Phi} - \left(A^\dagger - \frac{F^\dagger}{k}\right)\Psi^\dagger \,\middle|\, d\Phi \right\rangle + \left\langle \frac{\partial f}{\partial \Phi^\dagger} - \left(A - \frac{F}{k}\right)\Psi \,\middle|\, d\Phi^\dagger \right\rangle + \\ &+ \left\langle \frac{\partial f}{\partial \Sigma} \,\middle|\, d\Sigma \right\rangle - \left\langle \Psi^\dagger \,\middle|\, \left(dA - \frac{dF}{k}\right)\Phi \right\rangle - \left\langle \Psi \,\middle|\, \left(dA^\dagger - \frac{dF^\dagger}{k}\right)\Phi^\dagger \right\rangle \\ &- \frac{dk}{k^2}\left(\left\langle \Psi^\dagger \,\middle|\, F\Phi \right\rangle + \left\langle \Psi \,\middle|\, F^\dagger\Phi^\dagger \right\rangle\right) \end{aligned} \tag{3.19}$$

The first two terms on the RHS vanish if we can find two functions Ψ and $\Psi^\dagger$ such that the following equations are satisfied:

$$\begin{aligned} \left(A^\dagger - \frac{F^\dagger}{k}\right)\Psi^\dagger = \frac{\partial f}{\partial \Phi} &\iff \left\langle \frac{\partial f}{\partial \Phi} \,\middle|\, \Phi \right\rangle = 0 \\ \left(A - \frac{F}{k}\right)\Psi = \frac{\partial f}{\partial \Phi^\dagger} &\iff \left\langle \frac{\partial f}{\partial \Phi^\dagger} \,\middle|\, \Phi^\dagger \right\rangle = 0 \end{aligned} \tag{3.20}$$

These equations hold if we use f as chosen, that is a homogeneous functional of degree zero. Indeed, for the Euler's theorem, given a homogeneous function f of degree n, i.e. $f(\lambda x) = \lambda^n f(x)$ for every vector x, then $\left\langle \frac{\partial f}{\partial x} \,\middle|\, x \right\rangle = nf$.

However, the two Lagrange multipliers Ψ and $\Psi^\dagger$ are not unequivocally deter-

mined, indeed $\Psi - \lambda\Phi$ and $\Psi^\dagger - \lambda^\dagger\Phi^\dagger$ are also solutions of the same problem for every scalar λ and $\lambda^\dagger$. Starting from the particular solutions Ψ_0 and $\Psi_0^\dagger$, λ and $\lambda^\dagger$ are chosen in such a way that the last term in $\frac{dk}{k^2}$ of the Equation 3.19 vanish:

$$\begin{aligned} &\text{defining } \Psi = \Psi_0 - \lambda\Phi, \text{ if } \lambda = \frac{\left\langle \Phi^\dagger \,\middle|\, F\Psi_0 \right\rangle}{\left\langle \Phi^\dagger \,\middle|\, F\Phi \right\rangle} \implies \left\langle \Psi \,\middle|\, F^\dagger\Phi^\dagger \right\rangle = 0 \\ &\text{defining } \Psi^\dagger = \Psi_0^\dagger - \lambda^\dagger\Phi^\dagger, \text{ if } \lambda^\dagger = \frac{\left\langle \Psi_0^\dagger \,\middle|\, F\Phi \right\rangle}{\left\langle \Phi^\dagger \,\middle|\, F\Phi \right\rangle} \implies \left\langle \Psi^\dagger \,\middle|\, F\Phi \right\rangle = 0 \end{aligned} \tag{3.21}$$

Therefore, Equation 3.19 becomes:

$$df = \left\langle \frac{\partial f}{\partial \Sigma} \,\middle|\, d\Sigma \right\rangle - \left\langle \Psi^\dagger \,\middle|\, \left(dA - \frac{dF}{k} \right) \Phi \right\rangle - \left\langle \Psi \,\middle|\, \left(dA^\dagger - \frac{dF^\dagger}{k} \right) \Phi^\dagger \right\rangle \tag{3.22}$$

The first term on the RHS is called *direct term*, and it represents how the change of the cross-section affect directly the functional f. The last two terms are called, instead, *indirect terms*. They take into account the functional f variation due to the change of Φ and $\Phi^\dagger$, caused by the cross-section perturbation.

3.5.2 Discretization

Since with a computer it is more difficult to deal with continuos variables, the fields, such as the flux and the importances, are not defined with a function for each point of the space, rather by an average value for each small volume of the reactor. In addition, concerning the energy, we have applied the so-called *multi-group approximation*. It involves dividing the neutron energy spectrum into a discrete set of energy groups and treating neutrons within each group as having a representative energy and cross-section value. In this work of thesis, we have used the 33 groups available in the simulation software ERANOS [19] which are a good comprise between calculation time and results' accuracy.

This implies that we have available a value of the flux, adjoint and cross-section for each group (energy discretization) and for each fuel assembly (spatial discretization). It is common to apply this approximation. The thing that is possible to do, without changing the structure of the algorithm, is to increase the number of groups and the number of *volume cell*. This would provide us more precision at the cost of more CPU-time.

Nonetheless, 33 groups are sufficient to cause some computational issue: in the Equations 3.17 and 3.22, that are needed to compute the fit function, the featured

inner products include also the integration all over the energies. These calculations can be done directly in the fit function as it had been done in a first moment, but the computational time of the tool exploited for the optimization increased significantly. To achieve a better result in terms of computational time, it is possible to reduce the number of operations needed by performing in advance the energy integral, while preserving the original energy integral in the computation of the fit function. This can be obtained by defining a new set of cross-sections

$$\tilde{\Sigma}_i^j = \frac{\sum_g \phi_{ig}\phi_{ig}^\dagger \Sigma_{ig}^j}{\varphi_i} \tag{3.23}$$

where i, j and g represent respectively the fuel assembly, its residence time in the core and the group of energy and $\varphi_i = \sum_g \phi_{ig}\phi_{ig}^\dagger$. If we use this new set, that has a smaller cardinality than the original one, because we have a value for each fuel assembly and for each instant of the full cycle that we have considered, but not for each group, we reduce drastically the computational time exploited by the optimization tool. Given this definition, all the terms that contain the inner product are re-defined with the new value of the cross-section and a new inner product that does not include the energy integration. As example, the expression

$$\left\langle \Phi(\mathbf{r}, E) \,\middle|\, \delta\nu\Sigma_f^j(\mathbf{r}, E)\Phi^\dagger(\mathbf{r}, E) \right\rangle$$

becomes the sum

$$\sum_i^{N_{FA}} \delta\nu\tilde{\Sigma}_{f_i}^j \varphi_i$$

that is equivalent to perform the original integral given how we have defined the new set of cross-section.

3.6 Model of the problem

At the beginning of this Chapter, we have seen that to find a good distribution of fuel assemblies keeps the reactivity as constant as possible between the cycles and avoids big power clusters in the reactor core. In order to find the best distribution in batches, it is inconvenient recomputing exactly the whole reactor state (i.e. the reactivity and the power distribution) for each single trial distribution, as there could be thousands of distribution and it would take too much time. Therefore, it is possible to exploit the *standard perturbation theory* and the *generalized perturbation*

theory to compute respectively the variation of the reactivity and of the functional that represents the power distribution with respect to a reference state.

The reference state that have been considered in this work of thesis is the one in which all the fuel elements belong to the same batch and they all contain fresh fuel.

Reactivity With the Equation 3.17, it is possible to determine the variation of the reactivity of a certain distribution in batches with respect to the reference configuration. The variation has been computed for two of the most important instants of the cycle, BoC and EoC. In addition, since there is a number of cycles equals to the number of batches, it is possible to compute this variation for each selected instant, BoC and EoC, for each cycle by performing the batches' rotation. That consists in computing the reactivity variation by using the cross-section corresponding to the residential time of that particular fuel assembly into the core and using the flux and importance of BoC or EoC.

Power distribution The same is valid to compute the variation of the power functional with Equation 3.22. While for the reactivity we have already the expression of the variation, for the power distribution it is necessary to define the functional it is represented by. We have to think about how the power is distributed. We can assume that if the temperature limits are not exceeded in the hottest elements at a certain instant of time, we can expect the same in all the other elements. Given the reactor design, the neutron flux is distributed with a peak in the center of the core because of the physics of neutrons transport, so the hottest elements are also in this region (Section 2.4). This is true at BoC, while at EoC the power and temperature distribution could change, and the hottest elements could not be anymore the central ones. For this reason, we can fix the *detector* and define the *generalized importance* as the contribution to the total power of the sum of the power of these groups of elements. Let us call these groups of fuel assemblies, one for BoC and one for EoC, *reference assemblies*. It is important to understand that the functional f (defined just below) should refer to the fuel assembly that produce more power but, since it is very complicated to develop this model, it has been made the simpler choice. The second-best solution was to consider the importance of the hottest assemblies within the group of hottest elements (since we usually know where the hottest element can be) independently but, again, the model would have been too complicated. For this reason, we have considered the sum of the assemblies that

contain the hottest one.

The functional f of the power can be defined as

$$f = \frac{\Delta P}{P} \tag{3.24}$$

where ΔP is the variation of P with respect to the reference state in which all the fuel assemblies belong to the same batch, and P is the measure of how much the power of the *reference assemblies* contribute to the total power defined as

$$P = \frac{\iiint_{V_{ref}} \alpha \Sigma_f(\mathbf{r}, \mathbf{\Omega}, E) \Phi(\mathbf{r}, \mathbf{\Omega}, E) \, \mathrm{d}V \, \mathrm{d}\mathbf{\Omega} \, \mathrm{d}E}{\iiint \alpha \Sigma_f(\mathbf{r}, \mathbf{\Omega}, E) \Phi(\mathbf{r}, \mathbf{\Omega}, E) \, \mathrm{d}V \, \mathrm{d}\mathbf{\Omega} \, \mathrm{d}E}$$

where α is the energy produced for each fission reaction, that is about 200 MeV, and the integral in $\mathrm{d}V$ in the numerator is only on the volume of the *reference assemblies*, while the one at the denominator is on the full volume of the core. Note that P and ΔP are dimensionless quantities.

Given this definition of the functional, it is clear that the Equation 3.22 becomes simpler, since the last term on the RHS is not present anymore because of Equation 3.20 and from the fact that the power does not depend on the adjoint flux.

3.6.1 Goodness of a distribution

Now that we have the expression of the effect of the perturbation for both the reactivity and the power, it is possible to proceed with the determination of a *fitness function* that allows to measure the goodness of a configuration. There are several possibilities in the choice of the metric, but in the development of the algorithm it has been chosen one of the simplest: the square deviation from the mean value. This means that the change in the reactivity and in the power distribution is computed for each instant of the cycle, for both BoC and EoC. Then the square deviation from the mean values is computed for each quantity and for both BoC and EoC as in the following Equation

$$\begin{aligned} &\sum_{i=1}^{N_b} \left| \delta\rho_i^{BoC} - \overline{\delta\rho}^{BoC} \right|^2 + \left| \delta\rho_i^{EoC} - \overline{\delta\rho}^{EoC} \right|^2 + \\ &+ \left| \delta \left(\frac{\Delta P}{P} \right)_i^{BoC} - \overline{\delta \left(\frac{\Delta P}{P} \right)}^{BoC} \right|^2 + \left| \delta \left(\frac{\Delta P}{P} \right)_i^{EoC} - \overline{\delta \left(\frac{\Delta P}{P} \right)}^{EoC} \right|^2 \end{aligned} \tag{3.25}$$

where N_b is the number of batches. Given this fitness function, the lower the value, the better is the distribution.

3.6.2 Approximations

For the sake of simplicity and to reduce the computational time to run the algorithm, some approximations have been made in order to compute the effects of the perturbation. Here, these approximations, in addition to the first order approximation for the perturbation theory, will be shown.

Neglection of leakage and scattering As we have already said, the transport equation is a balance between production and loss of neutrons and it considers several types of process, such as the elastic and inelastic scattering, the leakage, and the production of neutron other than fission. In the frame of the perturbation theory, what matters are the variation of the cross-section and if we consider just the effects of the variations of fission and absorption cross-sections, we are able to explain the 99.2% of the total variation of the reactivity, as we can see from Table 3.1. A similar percentage can be obtained to explain the variation of the power functional. Therefore, it is possible, with good approximation, to consider the cross-sections variations other than the one for fission and absorption, as null. So, in the Equation 3.17 the scattering and leakage terms vanish. This allows also to substitute the *angular flux* with the *scalar flux*, that is independent of the angle. Indeed, since there is not any cross-section term that depends on the angle, it is possible to integrate separately the flux and its adjoint all over the angles. This is an advantage concerning the computational time, indeed this calculation can be performed only once at the beginning of the program.

Correlation space-energy The equations written above include inner products, that mathematically correspond to integrals on energy and on the space. In order to keep the model simple as a starting point, we performed the integrals of the inner products separately. Specifically, the inner product which regards three terms, the flux, its adjoint and the cross-sections, has been computed for its space part separately for the three quantities, and then it has been made the energy integral on their product. In other words, it has been computed the product of the space integrals of flux, adjoint and cross-section instead of the integral of their product. From the equations and from the result we can see that this approximation is the major source of error with respect to the other ones, but, in any case, we are able

Capture	$-5.303 \cdot 10^{-03}$
Fission	$-3.626 \cdot 10^{-02}$
Fission spect.	$5.746 \cdot 10^{-05}$
Transport	$2.482 \cdot 10^{-04}$
Elastic	$-3.293 \cdot 10^{-04}$
Inelastic	$-2.765 \cdot 10^{-04}$
(n, xn)	$-1.460 \cdot 10^{-05}$
Sum	$-4.188 \cdot 10^{-02}$

Table 3.1. Here are reported the contribution to the reactivity variation for the different terms, for the test-case reactor, ALFRED. If we consider just the *capture* and *fission* terms, we get a reactivity variation of $-4.156 \cdot 10^{-02}$, that corresponds to 99.2% of the total variation if we consider all the terms. The values reported have been computed through ERANOS that applied the first-order perturbation theory without any approximation.

to obtain acceptable results for this preliminary investigation.

History effect The macroscopic cross-sections of each fuel assembly depend on how many fissile atoms are present in the fuel and that changes accordingly on how much it has been burnt in the past; the burning of a fuel assembly also depends on which assemblies are present around it. That means that the cross-sections of each element, at a certain instant of time, depend on its own and its neighbors' history. Since we do not know a priori to which batch a fuel assembly belongs to, we have generated the cross-section in the reference case in which all the fuel assemblies belong to the same batch. Thus, the used cross-sections take into account the history of the neighbors in this reference case and not in the case of the found distribution. We expect this approximation to be small, due to the fact that each batch of a typical distribution, as we will see, is homogeneously spread on the core map.

Chapter 4

Structure of the Optimization Algorithm

In this Section, it will be discussed the structure of the developed optimization algorithm. We have followed two different paths to get the best distribution of fuel assemblies into batches: an analytical optimization, and a genetic one. It will be presented an overview of the structure of the developed algorithm and the working principle of these two optimization algorithms. The algorithm has been written and runs with Python 3.10.8, exploiting the Pyomo library [20] [21] for the analytical optimization and a `C++` API developed by Mattia Massone[1] for the genetic algorithm. The genetic algorithm, even if it is written in `C++`, computes the value fitness function in Python. This is possible exploiting the library `pybind` [22], that allows to use in `C++` script already written in Python and vice versa.

4.1 General procedure

In Figure 4.1, it is reported the flowchart that shows schematically the structure of the algorithm. As first step it is present the reading of all the necessary files. Among these, we find a configuration `yaml` file, written by the user, that includes all the information needed like:

- the number of batch in the reactor fuel cycle,
- the number of assemblies,
- information about the active region and

[1] PhD, ENEA-Agenzia nazionale per le nuove tecnologie, l'energia e lo sviluppo economico sostenibile.

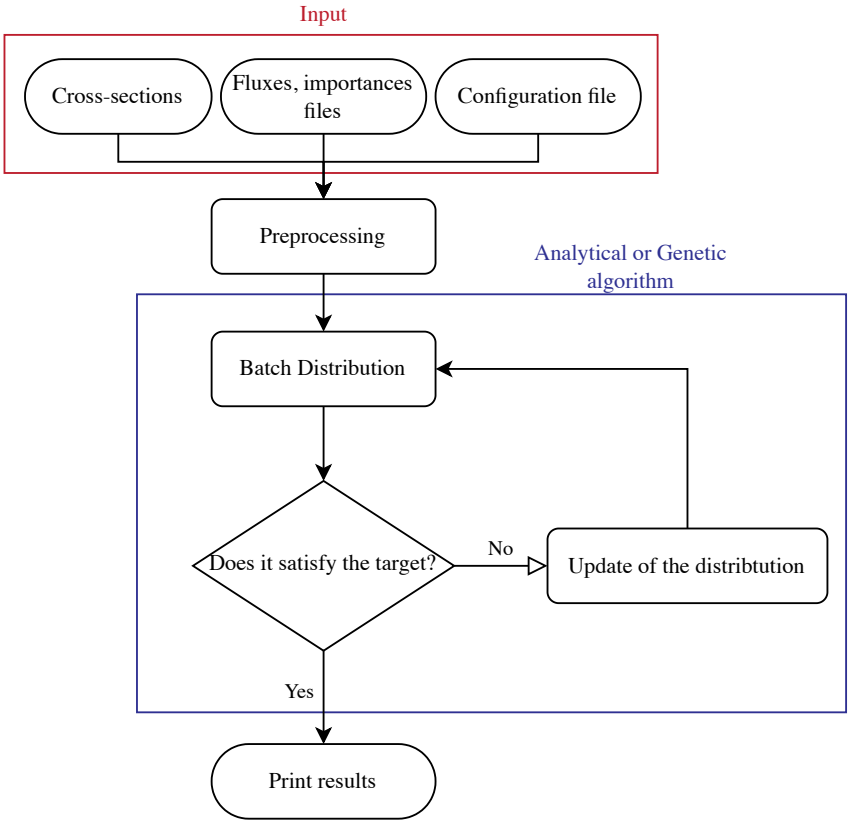

Figure 4.1. Flowchart of the developed algorithm.

- the reference assemblies for the generalized power importance at BoC and EoC.

In this phase also the files containing the cross-sections, fluxes and the importances generated by the simulations are read (Section 4.1.2). After the reading, it is necessary to make a preprocessing phase (Section 4.1.3), in which the data are compressed from a three-dimensional to a two-dimensional space.

After the preprocessing phase, the analytical or the genetic algorithm starts to operate. As we will see, these two algorithms work in different manners, but we can say that the working principle is the following: the fit function is computed for a given batch distribution and it is then updated according to certain criteria until its value achieves a target predefined value, or another termination condition is satisfied.

Ultimately, some output and images are printed to show the results of the optimization.

4.1.1 Cross-section treatment

As input, we have a file for the cross-sections. The file includes a cross-section set for each energy group, fuel enrichment, and time instant of the cycle. These values have been generated by the *European Reactor ANalysis Optimized calculation System* (ERANOS) [19] software, with the *one-batch approximation* and with the control rods fixed in an intermediate (median) position between BoC and EoC.

4.1.2 Reading of the fluxes and importances

The first step of the algorithm consists in the reading of the fields, such as the fluxes, the importances and the generalized importances, at BoC and EoC. The fluxes and importances have been generated by ERANOS, solving the transport equation on a three-dimensional hexagonal model with 33 groups of energy with the library `ENDF/B-VIII.0` [23]. For some limits o f ERANOS, it was not possible to generate with a 3D model also the generalized importances, that have been generated using a diffusion model instead of a transport one. However, it has been verified that the introduced error was acceptably small.

The products of these full simulations have been then stored into *Medcoupling* files. *Medcoupling* is a SALOME [24] library for processing meshes and fields that allows, among the other things, to analyze them. Each file contains a three-dimensional *mesh* and a *field* (Figure 4.2). The first one is a collection of *nodes* and *cells* that defines the structure of the region of interest and divides it into smaller volumes. The *field*, instead, is composed by the values of the flux, importance or generalized importance in each cell of the *mesh*. In a file, there could be more than one set of values for each *field*, one for each energetic group.

In Figure 4.2, around the fuel assemblies, other subassemblies are present in order to simulate the material around the core, and get the field also in this region. Since they do not have any effect on the relevant quantities of the problem, in this work of thesis, they have not been considered.

4.1.3 Preprocessing

Once the Medcoupling files have been read, it is possible to exploit the *space-energy correlation* approximation (Section 3.6.2) to integrate over the volume along the axial region. In this process, only the cells in the active region have been considered.

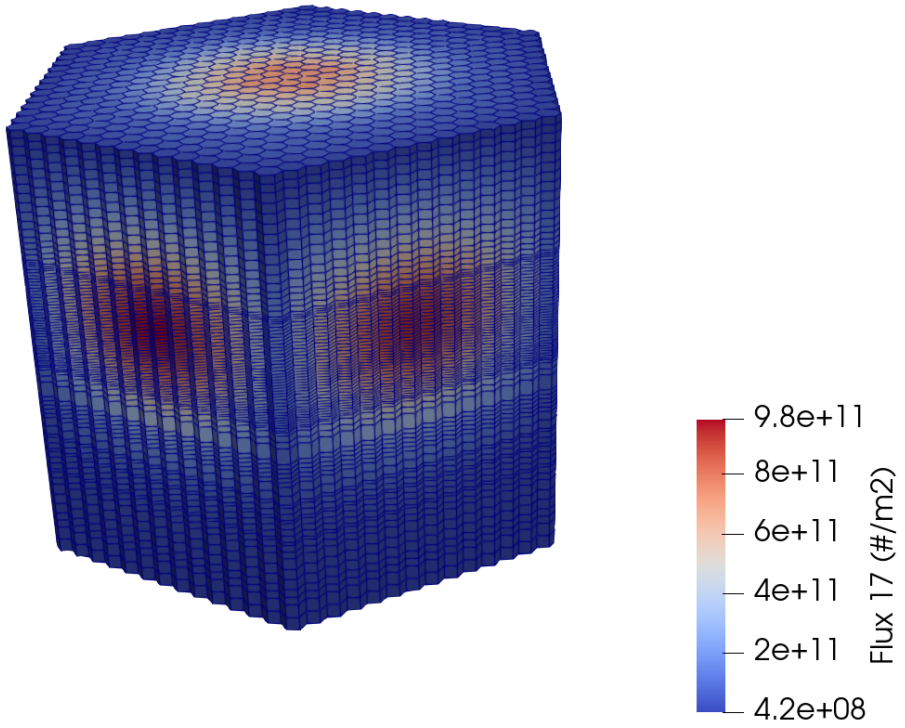

Figure 4.2. Example of data contained in the Medcoupling files. It is possible to recognize the three-dimensional mesh (the blue grid) and the field corresponding to the colors.

Since the mesh is made by discrete cells, the integral is computed as a summation:

$$\phi_{ig} = \frac{\sum_{j=1}^{N_{cell}} \phi_{igj} V_{ij}}{\sum_{j=1}^{N_{cell}} V_{ij}}$$

where ϕ_{ig} indicates the integrated final flux of i-th fuel assembly of the g-th group, and ϕ_{igj} the flux of the j-th cell of the i-th fuel assembly of the g-th group, N_{cell} is the number of cells axially present in the active region and V_{ij} the volume of the j-th cell of the subassembly i. In that way, from a three-dimensional structure of the field, we achieve a two-dimensional one. This process is repeated for each group of the field.

Regarding the cross-sections, new sets of cross-sections, one for each functional and instant of the cycle, have been created according to Equation 3.23 to speed up the optimization process.

4.1.4 Computation of the fit function

The fitness function expression is given by Equation 3.25. In the case the user would like to prioritize the optimization of a parameter over another, or at BoC over EoC, we have introduced four *scaling factors* that multiply each term of the fit function. In this work of thesis some experiments (Appendix A) have been carried out with different values of these parameters, but in the end only the case where both reactivity and power distribution contribute equally to the fit function has been considered (i.e. with the same *scaling factors*). Also the scaling factors that prioritize the optimization at a certain instant of time have been set to the same value; indeed, there is not any engineering reason to prefer one instant over the other.

4.2 Analytic Algorithm

4.2.1 Problem formulation

In order to model the problem, we have taken the inspiration from the approach of [25] by introducing the characteristic function

$$\xi_{ij} = \begin{cases} 1 & \text{if the element } i \text{ belongs to the batch } j \\ 0 & \text{otherwise} \end{cases}$$

for $i = 1 \dots N_b$ and $j = 1 \dots N_{FA}$, where N_b is the number of batches and N_{FA} the number of fuel assemblies. Since it is not possible to assign a fuel assembly to more than one batch, we have that the problem is subjected to the constraints:

$$\sum_{j=0}^{N_b} \xi_{ij} = 1 \qquad \forall\ i = 1, \dots N_{FA}$$

To summarize, we have that our optimization problem can be written as:

$$\begin{aligned} &\min_{\xi}\ f(\xi) \\ &\text{s.t.} \sum_{j=0}^{N_b} \xi_{ij} = 1 \qquad \forall\ i = 1, \dots N_{FA} \end{aligned} \tag{4.1}$$

where $f(\xi)$ is the fit function of Equation 3.25, in which the terms $\delta\rho$ and $\delta\frac{\Delta P}{P}$ are:

$$\delta\rho = \frac{\sum_{j=1}^{N_b}\sum_{i=1}^{N_{FA}} \phi_i\phi_i^\dagger\xi_{ij}\left(\frac{\delta\nu\Sigma_{f_i}^{(j)}}{k_{eff}} - \delta\Sigma_{a_i}^{(j)}\right)}{\sum_{i=1}^{N_{FA}} \phi_i\phi_i^\dagger\nu\Sigma_{f_i}^{(1)}} \tag{4.2}$$

$$\delta\frac{\Delta P}{P} = \sum_{j=1}^{N_b}\sum_{i=1}^{N_{FA}} \phi_i\phi_{p_i}^\dagger\xi_{ij}\left(\frac{\delta\nu\Sigma_{f_i}^{(j)}}{k_{eff}} - \delta\Sigma_{a_i}^{(j)}\right)V_i + \delta\Sigma_{p_i}\left(\frac{1}{P}\frac{\partial P}{\partial\Sigma_p}\right)_i \tag{4.3}$$

where k_{eff} is considered the one at the reference state (in accordance with the first order perturbation theory used), $\Sigma_p = \alpha\Sigma_f$, and α is the average energy produced per fission. The derivative of the direct term (Section 3.5.1):

$$\frac{1}{P}\left(\frac{\partial P}{\partial\Sigma_p}\right)_i = \frac{\phi_i\zeta_i}{\sum_{j=1}^{N_{FA}}\Sigma_{p_j}\phi_j\zeta_j} - \frac{\phi_i}{\sum_{j=1}^{N_{FA}}\Sigma_{p_j}\phi_j} \tag{4.4}$$

where ζ is the characteristic function:

$$\zeta_n = \begin{cases} 1 & \text{if the element } n \text{ is a reference assembly of the power} \\ 0 & \text{otherwise} \end{cases}$$

4.2.2 Solving method

The optimization problem above presented has been solved with a *Mixed Integer Non Linear Programming* (MINLP) method. MINLP problems are a subclass of optimization problems that combines the use of *Mixed Integer Linear Programming* (MILP) and of the *Non Linear Programming* (NLP) solvers. The problems of this category involve both integer and continuous variables, as well as non-linear functions. The characteristics of the MINLP allows modelling a vast number of real-world problems in different areas, such as engineering, finance, computational chemistry [26].

In this thesis it will be presented, after a brief introduction, just the algorithm of the Pyomo library exploited to solve the optimization problem.

The problem has been modeled as a convex MINLP, that is a subclass of the MINLP problems with the property of containing only convex functions. This assumption guarantees the convergence of the problem to a solution. [26]

A general MINLP problem can be written as:

$$\begin{aligned} &\min_{\mathbf{x},\mathbf{y}} \ f(\mathbf{x},\mathbf{y}) \\ &\text{s.t. } g_j(\mathbf{x},\mathbf{y}) \leq 0 \quad \forall j = 1,\dots l \\ &\quad \mathbf{A}\mathbf{x} + \mathbf{B}\mathbf{y} \leq \mathbf{b} \\ &\quad \mathbf{x} \in \mathbb{R}^n,\ \mathbf{y} \in \mathbb{Z}^m \end{aligned} \tag{4.5}$$

where f is the function to be minimized, $\mathbf{x}$ and $\mathbf{y}$ are respectively the real and integer variables, g_j are the non-linear functions, called *constraints* and $\mathbf{A}\mathbf{x} + \mathbf{B}\mathbf{y} \leq \mathbf{b}$ is the linear constraint. As said above, it is important that $f, g_1, \dots g_l : \mathbb{R}^n \times \mathbb{Z}^m \to \mathbb{R}$ are convex and continuously differentiable.

To obtain a solution to the problem, different approaches can be used. Let us analyze the ones used in this work of thesis.

Outer Approximation The *Outer Approximation* [27] is an algorithm to obtain the optimal solution to the original problem by solving a sequence of MILP and NLP sub-problems and finding a polyhedral representation of the *feasible space* of solutions. This method uses a linear approximation of the MINLP original problem.

The *Outer Approximation* starts with the relaxed solution of the original problem, in which the domain of the integer variables is extended to $\mathbb{R}$.

At iteration k, the next integer combination $\mathbf{y}^{k+1}$ is obtained by solving the following MILP sub-problem with the introduction of a variable μ:

$$\begin{aligned} &\min_{\mathbf{x},\mathbf{y},\mu} \ \mu \\ &\text{s.t. } f(\mathbf{x}^i,\mathbf{y}^i) + \nabla f(\mathbf{x}^i,\mathbf{y}^i)^T \begin{bmatrix} \mathbf{x}-\mathbf{x}^i \\ \mathbf{y}-\mathbf{y}^i \end{bmatrix} \leq \mu \quad \forall\ i = 1,\dots k, \\ &\quad g_j(\mathbf{x}^i,\mathbf{y}^i) + \nabla g_j(\mathbf{x}^i,\mathbf{y}^i)^T \begin{bmatrix} \mathbf{x}-\mathbf{x}^i \\ \mathbf{y}-\mathbf{y}^i \end{bmatrix} \leq 0 \quad \forall\ i = 1,\dots k, \quad \forall\ j \in \mathcal{I}_i \\ &\quad \mathbf{A}\mathbf{x} + \mathbf{B}\mathbf{y} \leq \mathbf{b} \\ &\quad \mathbf{x} \in \mathbb{R}^n,\ \mathbf{y} \in \mathbb{Z}^m,\ \mu \in \mathbb{R} \end{aligned} \tag{4.6}$$

where $\mathcal{I}_i$ is the set of the index of the non-linear constraint active at the trial solution $(\mathbf{x}^i, \mathbf{y}^i)$. Since the feasible set is overestimated and the objective is underestimated, because of the convexity of the problem, the optimum of this problem provides a good lower bound for the original MINLP problem. Actually, we do not solve

exactly this problem, but a slightly different one, because of the regularization that will be explained in the following paragraph.

Once the new integer combination $\mathbf{y}^{k+1}$ is obtained, we can determine the corresponding $\mathbf{x}$ variables by solving the convex NLP sub-problem:

$$\begin{aligned} \min_{\mathbf{x}} \; & f(\mathbf{x}, \mathbf{y}^{k+1}) \\ \text{s.t. } & g_j(\mathbf{x}, \mathbf{y}^{k+1}) \leq 0 \quad \forall\, j = 1, \dots l, \\ & \mathbf{A}\mathbf{x} + \mathbf{B}\mathbf{y}^{k+1} \leq \mathbf{b} \\ & \mathbf{x} \in \mathbb{R}^n \end{aligned} \tag{4.7}$$

If this problem can be solved to optimality, we obtain $\mathbf{x}^{k+1}$, that provides us a valid upper bound to the original MINLP problem. If, instead, the problem is infeasible, we can get the $\mathbf{x}$ variables by solving a feasibility problem, that minimizes the constraint violation with the current choice of $\mathbf{y}$:

$$\begin{aligned} \min_{\mathbf{x},r} \; & r \\ \text{s.t. } & g_j(\mathbf{x}, \mathbf{y}^{k+1}) \leq r \quad \forall\, j = 1, \dots l, \\ & \mathbf{A}\mathbf{x} + \mathbf{B}\mathbf{y}^{k+1} \leq \mathbf{b} \\ & \mathbf{x} \in \mathbb{R}^n,\ r \in \mathbb{R}_+ \end{aligned} \tag{4.8}$$

By solving the feasibility problem, we can get the continuous variables $\mathbf{x}^{k+1}$. If $(\mathbf{x}^{k+1}, \mathbf{y}^{k+1})$ is not a feasible solution, then we cannot get any upper limit at this iteration. Until the differences between the upper and lower bound is not within the predefined tolerance, we add new linearization (*cutting planes*) to the problems. These cutting planes are given by:

$$\begin{aligned} f(\mathbf{x}^{k+1}, \mathbf{y}^{k+1}) + \nabla f(\mathbf{x}^{k+1}, \mathbf{y}^{k+1})^T \begin{bmatrix} \mathbf{x} - \mathbf{x}^{k+1} \\ \mathbf{y} - \mathbf{y}^{k+1} \end{bmatrix} \leq \mu, \\ g_j(\mathbf{x}^{k+1}, \mathbf{y}^{k+1}) + \nabla g_j(\mathbf{x}^{k+1}, \mathbf{y}^{k+1})^T \begin{bmatrix} \mathbf{x} - \mathbf{x}^{k+1} \\ \mathbf{y} - \mathbf{y}^{k+1} \end{bmatrix} \leq 0, \quad \forall\, j \in \mathcal{I}_{k+1} \end{aligned} \tag{4.9}$$

and they will not exclude any feasible solution due to the convexity of the problem, but they remove the solutions that have been already encountered in the previous iterations.

The outer approximation can be summed up in the following pseudocode [27]:

1. Define the optimality tolerance $\epsilon > 0$.

2. Initialization.

   (a) Obtain a relaxed solution by solving an integer relaxation of MINLP problem.

   (b) Generate cutting planes according to Equation 4.9 for the point found in the previous step and building the problem of Equation 4.6.

   (c) Set the iteration counter: $k = 0$ and the upper and lower bounds respectively to $+\infty$ and $-\infty$.

3. Repeat until the distance between the upper (UB^{k-1}) and the lower bound (LB^{k-1}) is $\leq \epsilon$.

   (a) Solve the problem of Equation 4.6 to obtain $\mathbf{y}^k$ and the lower bound, LB^k.

   (b) Solve the problem of Equation 4.7 with fixed integer variables $\mathbf{y}^k$ to obtain $\mathbf{x}^k$.

   (c) If the problem 4.7 is infeasible, solve the feasibility problem of Equation 4.7 to get $\mathbf{x}^k$. Then set $UB^k = UB^{k-1}$.

   (d) Generate cutting planes according to Equation 4.9 and add them to the problem of Equation 4.6.

   (e) If $\mathbf{x}^k$, $\mathbf{y}^k$ is a feasible solution, then set $UB^k = \min\{f(\mathbf{x}^k, \mathbf{y}^k), UB^{k-1}\}$.

   (f) Increase the counter $k = k + 1$.

4. Return the best solution.

In our problem, we do have neither non-linear constraint nor real variables $\mathbf{x}$, thus, the algorithm is simpler with respect to the one above reported. For example, if the MILP problem is feasible, the same will be true for the NLP, since there are no non-linear constraints.

In Figure 4.3 it is possible to see how the *Outer Approximation* works with an example. The first iterations do not lead to any feasible solution, while in the fifth one we get it. The found solution is the optimal one, but another iteration is necessary to verify the optimality.

An overview of the *Outer Approximation* is given in the flowchart reported in Figure 4.4, that summarizes the main steps performed by the algorithm.

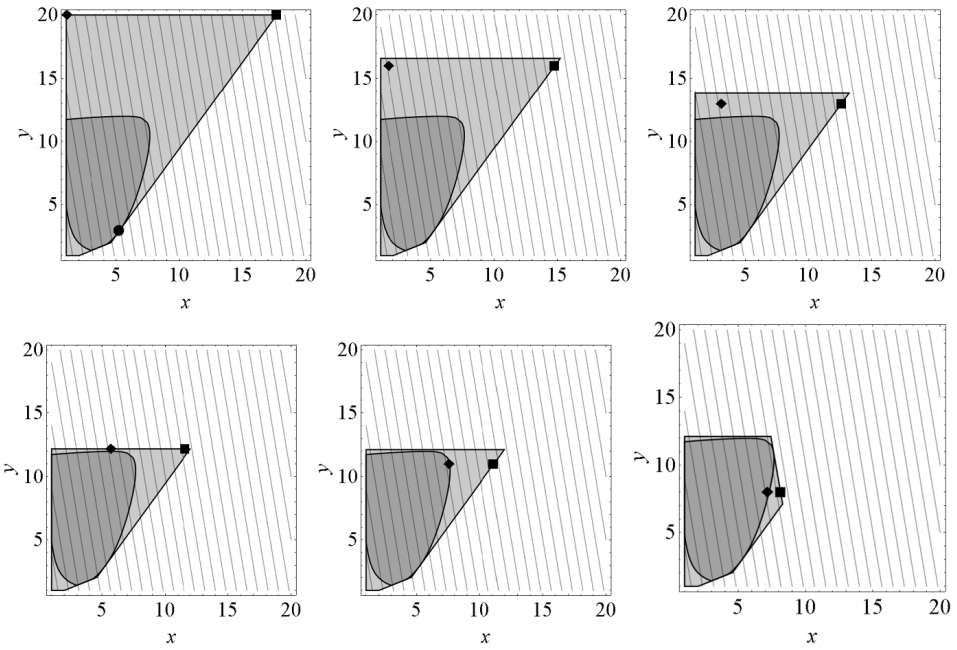

Figure 4.3. In this Figure it is possible to see how the *Outer Approximation* works with an example. Here are reported the first six iterations. In dark gray, it is represented the feasible region defined by the non-linear constraints. In light gray areas shows the *Outer Approximation* and the relatives cuts. The square dots are the solution from the MILP sub-problems, while the diamond shape ones are the solutions obtained from the NLP sub-problems. The dot in the first image represent the starting point [27].

Branch and Bound The *Branch and Bound* [26] approach is a method to solve the MILP problem of the Outer Approximation. The result is $(\mathbf{x}^k, \mathbf{y}^k)$, where k is the k-th iteration. It is the so-called *feasible solution* or *lower bound* for the original problem. If the $\mathbf{y}$ solution is made of integer values, then we have found the desired solution for the MILP, otherwise the problem is divided into two *branches*, which are two NPL problems in which, in addition to the original constraints, there are also, for a given i corresponding to a non-integer y^k, $y_i \leq \lfloor y_i^k \rfloor$ and $y_i \geq \lceil y_i^k \rceil$, respectively; as many branches are created as non-integers y_i^k. Once these sub-problems have been solved and we get another *relaxed solution* for each branch, we repeat the process: if one of the solutions is an integer solution, we may have found the best integer solution of that problem, otherwise we keep creating new branches and adding new constraint for each sub-problem. The formation of new branches ends when it has been found the best integer solution or the sub-problem has been declared *unfeasible*, that is, when the set of possible solutions given the constraints becomes empty.

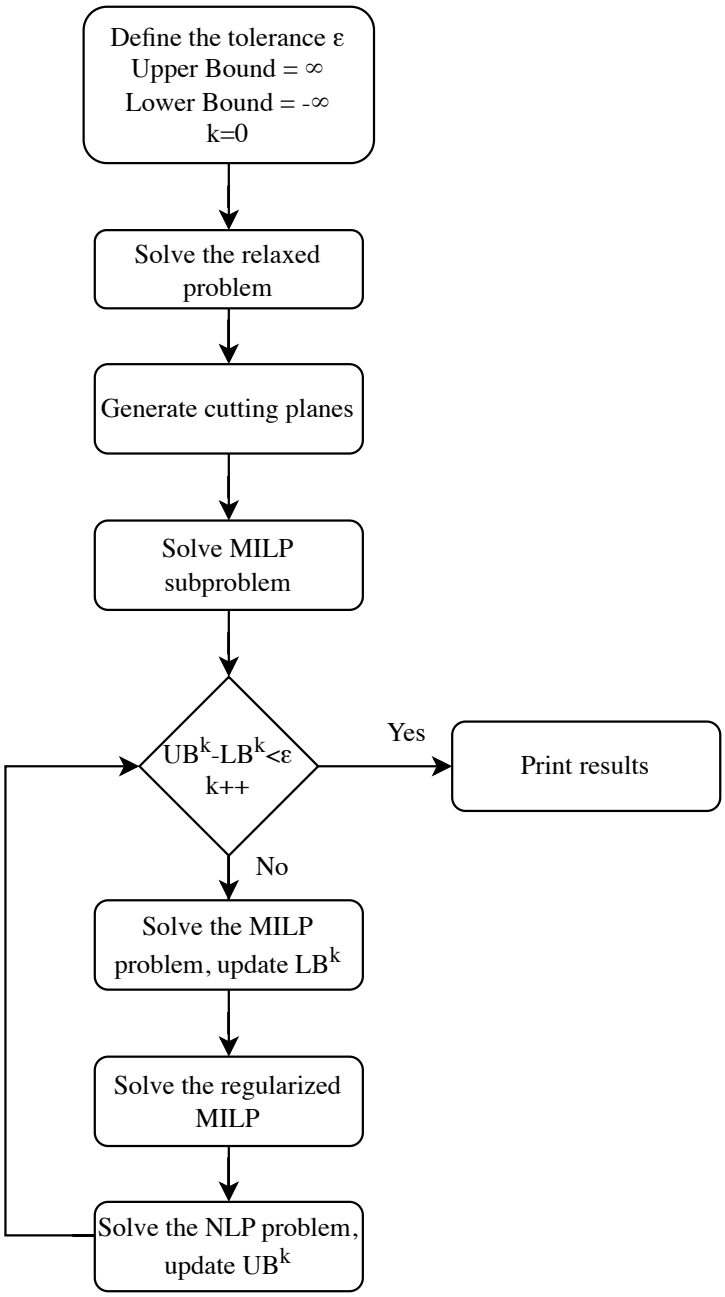

Figure 4.4. Flowchart reporting the main steps performed by the analytical optimization.

Regularization In order to obtain better integer solutions, it is possible to add a *regularization* to the model. The Pyomo toolbox offers several types of regularization, but here the Hessian one [27] has been exploited. It is useful to get information about the curvature of the constraints and the objective functions when choosing the integer combinations in order to make it easier to find the solution. For this reason, it is convenient to define and to use the Lagrangian function $\mathcal{L} : \mathbb{R}^n \times \mathbb{Z}^m \times \mathbb{R}^l \to \mathbb{R}$:

$$\mathcal{L}(\mathbf{x}, \mathbf{y}, \boldsymbol{\lambda}) = f(\mathbf{x}, \mathbf{y}) + \sum_{j=1}^{l} \lambda_j g_j(\mathbf{x}, \mathbf{y})$$

where $\lambda_j \geq 0$ is the Lagrange multiplier of the j-th non-linear constraint. The linear constraints are not considered, as they can be handled internally in the sub-problems. In this way it is possible to minimize the Lagrangian function in which the non-linear constraint are included, and subjected to the linear ones.

Minimizing just the Lagrangian is not useful because it does not bring any advantage with respect to the original problem, thus we have used a second order approximation:

$$\mathcal{L}(\bar{\mathbf{x}}, \bar{\mathbf{y}}, \bar{\boldsymbol{\lambda}}) + \nabla_{\mathbf{x},\mathbf{y}} \mathcal{L}(\bar{\mathbf{x}}, \bar{\mathbf{y}}, \bar{\boldsymbol{\lambda}})^T \begin{bmatrix} \Delta\mathbf{x} \\ \Delta\mathbf{y} \end{bmatrix} + \frac{1}{2} \begin{bmatrix} \Delta\mathbf{x} \\ \Delta\mathbf{y} \end{bmatrix}^T \nabla^2_{\mathbf{x},\mathbf{y}} \mathcal{L}(\bar{\mathbf{x}}, \bar{\mathbf{y}}, \bar{\boldsymbol{\lambda}}) \begin{bmatrix} \Delta\mathbf{x} \\ \Delta\mathbf{y} \end{bmatrix}$$

where $\nabla_{\mathbf{x},\mathbf{y}} \mathcal{L}$ is the gradient of the Lagrangian with respect to $\mathbf{x}, \mathbf{y}$, $\nabla^2_{\mathbf{x},\mathbf{y}}$ denotes the Hessian matrix, $\bar{x}, \bar{y}, \bar{\lambda}$ is the last point found nearest to the optimal solution and $\Delta\mathbf{x}$, $\Delta\mathbf{y}$ represent respectively $x - \bar{x}$ and $y - \bar{y}$.

By solving the MILP problem, we obtain an estimation of the LB^k therefore, we can define the expected best objective at the step k as:

$$f_k^* = (1 - \alpha) f(\bar{\mathbf{x}}, \bar{\mathbf{y}}) + \alpha LB^k$$

where $\bar{x}, \bar{y}$ is the best solution, $\alpha \in (\, 0, 1\,]$ is a parameter, fixed by the user, that evaluates where the real optimal solution is located: if it is nearer to the lower bound found by the MILP or to the best solution found until that moment. During the minimization of the regularized function, i.e. the Lagrangian, the Lagrangian, it is also useful to add the constraint $\mu \leq f_k^*$, that allows us to exclude all the solutions that provide a fit function worst than f_k^*. The result obtained from the optimization of the regularized problem is then passed to the NLP sub-problem.

In Figure 4.5 it is reported a graphical example of how the regularization works, with $\alpha = 0.5$. In this case, three iterations are needed, and the last one is just a

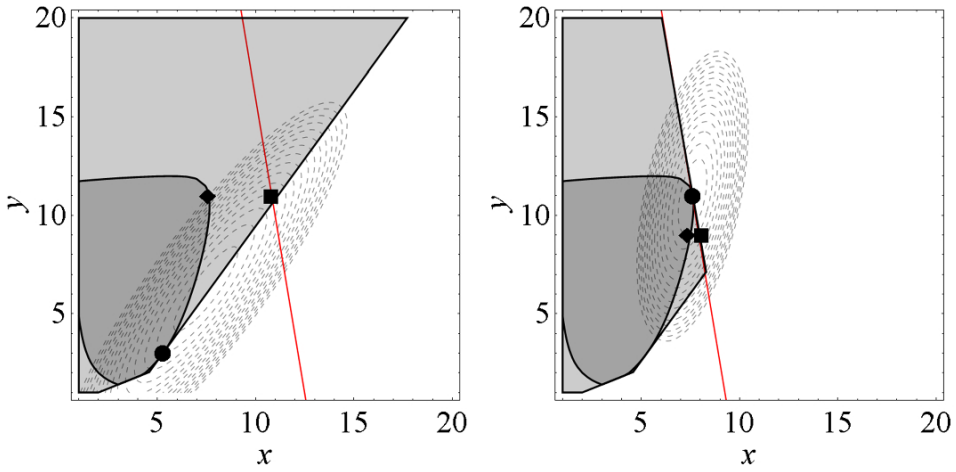

Figure 4.5. Example of how the regularization works. Here are presented the first two iterations needed to solve an optimization problem taken as example. The dashed ellipses represent the contours of the approximated Lagrangian, the red line shows the level constraint given by $\mu \leq f^*$. The circular dots represent the best found solution so far, the squared dots represent the solutions obtained from the regularized sub-problem and diamond shaped dots represent the solutions obtained by one of the NLP sub-problems. [27]

verification of the optimality, by solving the MILP problem.

4.3 Genetic Algorithm

The *genetic algorithms* are a family of meta-heuristic algorithms based on natural selection processes that allow to solve optimization problems by minimizing a fit function. To do that, they use certain techniques borrowed from natural evolution, such as *crossing over*, *mutations* and *selection*. The *genetic algorithms* are very useful to solve extremely complex problems that can be difficult to solve analytically. Despite that, it is not guaranteed the convergence of the fit function to the global minimum. Indeed, a too fast homogenization of the population would prevent its evolution, and the algorithm could become stuck at a local minimum. However, the *mutations*, as we will see, reduce the risk of this phenomenon.

Each candidate solution is called *individual* and a group of them is called *population*. Each *individual* has certain characteristics, that constitute its *genotype* or *chromosome*. Each *chromosome* is composed by several *genes*, at which we can assign different *alleles*. In our specific case, one *individual* is a batch distribution and the chromosome is the way we decided to represent the distribution, that is an array in which each *gene* correspond to a position in the core map. Each *gene* assumes a value equal to the number of the batch it belongs to (Figure 4.6).

The used genetic algorithm starts from a population of N_{pop} *individuals* whose fit function is computed. Once a series of genetic operators, that will be explained in the next paragraphs, has been applied to the population, we obtain a new *generation* of *individuals*. The new *generation* is composed by the same number of *individuals* as the original one, but it has, on average, better characteristics. This is the result of a *selection process*, which chooses the individuals of the current generation to be crossed and passed to the next one. The *selection process* uses some criteria, depending on the exploited algorithm, to choose the individuals with the best characteristics. Repeating this procedure iteratively leads to a population composed by individuals that, on average, better fit with the environment.

In the following paragraphs it will be described the main genetic operators used.

Tournaments selection The tournaments selection [28] (Figure 4.7) is one of the algorithms that performs a selection of individuals, and allows finding which couples of individuals have to be passed to the step of crossing over. Let us suppose to have a fixed number of tournaments, N_t. Each individual of the population of a generation is randomly assigned to a *tournament*. For each tournament, the best individual is chosen with a probability p, the second individual with a probability $p(1-p)$, the third one with a probability $p(1-p)^2$ and so on. Both N_t and p are needed to fine-tune the selection criteria of the algorithm. For example, if the tournament is big, that corresponds to a small N_t, a weak individual (i.e. with a small fitness function) in a tournament, has a low probability to be chosen, because there is a high probability that also a strong individual is in the tournament and that will be chosen from the selection. This would lead to a too fast homogenization of the population. On the contrary, if N_t is too big, there is a high chance that

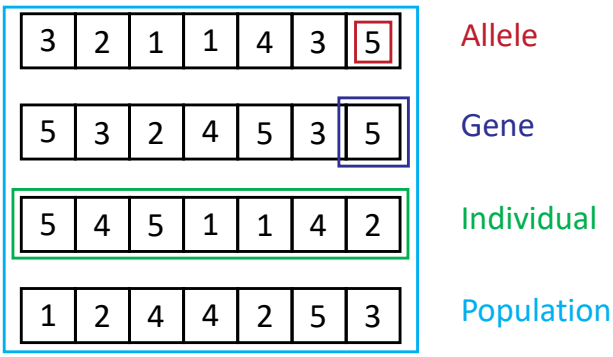

Figure 4.6. Graphic explanation of the nomenclature characteristic of the genetic algorithms.

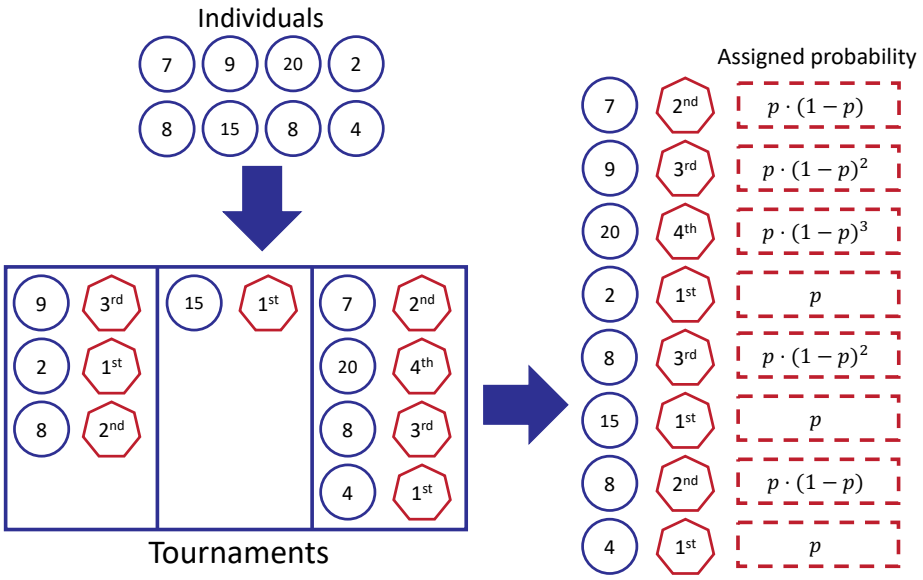

Figure 4.7. Graphic explanation of the tournament selection. Each individual is assigned randomly to one tournament. Then, a position in the ranking is assigned to each individual based on the fitness function value. Finally, a probability p is assigned to the first places, a probability $p(1-p)$ is assigned to the second places and so on. Figure inspired by [29].

a weak individual will be chosen. For this reason, it is always necessary to have a balance between the individual chosen and discarded.

Once the probability p has been assigned to each individual and re-normalized, it is possible to proceed with the crossing over.

Crossing Over The *crossing over* is an operator analogous to the biological sexual reproduction: two parents chromosomes produce two children that have a mixture of their parent's chromosomes. The couple of individuals undergoing *crossing-over* is chosen, each time, by randomly extracting them, according to the assigned probability in the tournaments selection. The *crossing over* can operate with different options (mainly depending on the chromosome representation), but in this case it has been used just the *single point crossover*. In Figure 4.8, it is possible to easily understand what the *single point crossover* consist in. Chosen a random *crossover point* that divides each chromosome into two parts, the children's chromosomes are generated by swapping the parts of the parents' chromosomes.

Mutation Given a certain individual, a *mutation* (Figure 4.9) consists in a random change of one random gene from an allele to another one. It is analogous to the

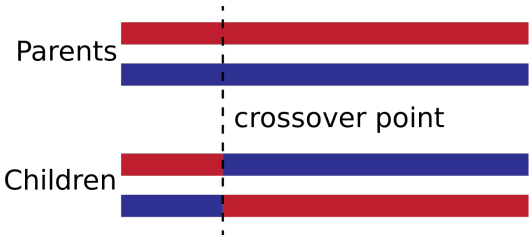

Figure 4.8. Graphic explanation of the *single point crossover*. The part on the left of the crossover point is swapped between the two chromosomes. [30]

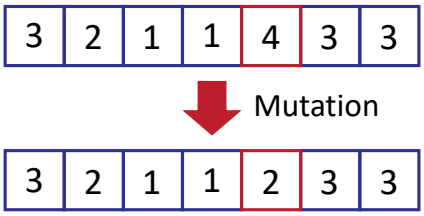

Figure 4.9. Graphic explanation of the *mutation* of a chromosome. In this case, there is only one *gene* which *allele* is mutated.

biological *point mutation*. In this problem, a mutation corresponds to movement of one element from a batch to another. The purpose of the mutations is to introduce diversity in the population and to reintroduce good characteristics of the chromosome that, for some reason, have disappeared in the previous generations. This prevents the algorithm from getting trapped near a local minimum and helps testing new individuals. In the code, it is possible to set a probability of mutation rate in population. For each individual, according to this parameter is decided whether it has a mutation or not. If it is the case, the number of mutation for that individual is extracted randomly from a Poisson's distribution with mean 2[2]. However, we have to pay attention to the value we set for the probability of mutation, because a value that is too high could make the genetic algorithm meaningless. Indeed, it would mean that most of the new individuals are subjected to mutation and that the trials we make to find the best individual are totally random. Therefore, it is necessary to balance the algorithm in order to introduce a bit of randomness but not enough to classify the algorithm as purely random.

Elitism Often, as in this case, it is used also the *elitism* operator. This operator guarantees that the best individuals of a generation have a place also in the next generation. Depending on the approach used by the algorithm, the elite individuals

[2]The mean of the Poisson's distribution will be modifiable in the future, but when we used it, it was fixed to this value.

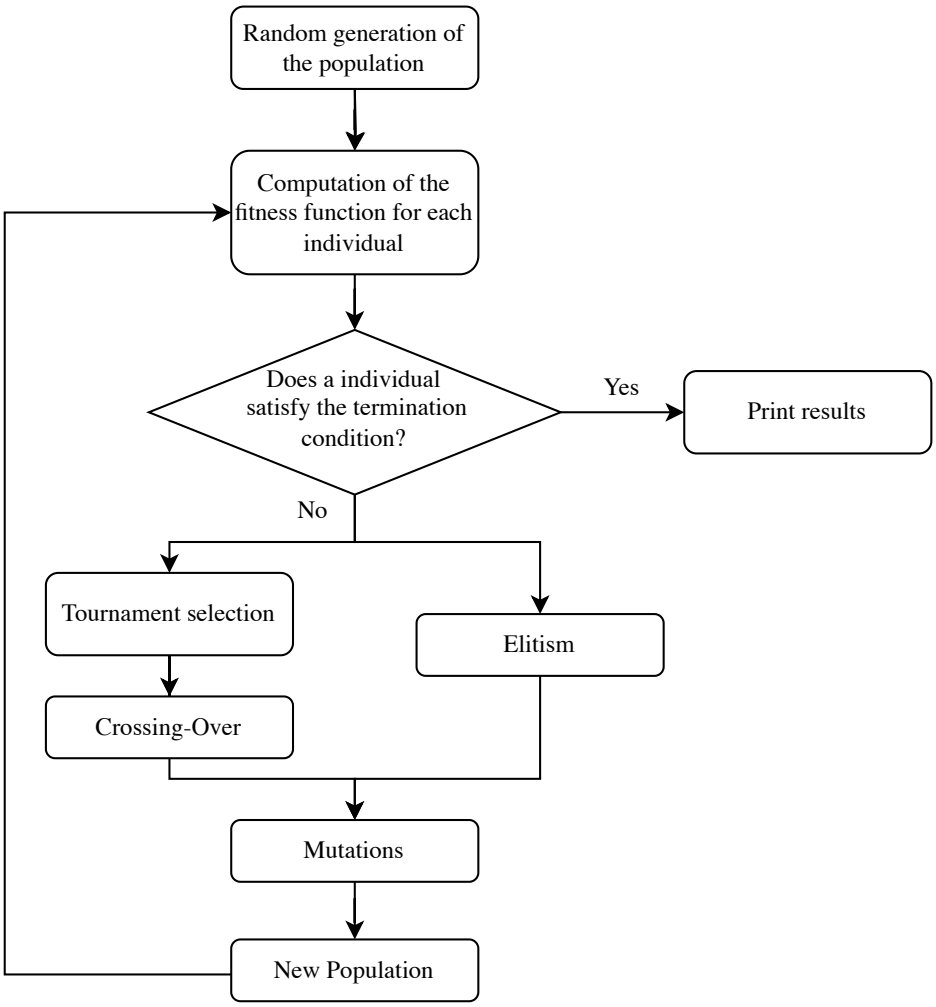

Figure 4.10. Flowchart summarizing how the genetic algorithm works.

can or cannot be subjected to mutation. In this case we opted for the first case, therefore an individual that is directly passed to the next generation, can be mutated. It is possible to fix a different percentage of the individuals that compose the next generation with a parameter.

All this process is repeated iteratively until a termination condition is satisfied. As termination condition, it is possible to use a limit value of the fitness function, a limit value for the average fitness function of the population, a maximum number of generations or a time limit.

In Figure 4.10 it is reported a flowchart that summarize the steps this algorithm perform to achieve the final result.

Chapter 5

Results of the optimization

The developed algorithm has been applied to the test case of the ALFRED reactor, that has been presented in Section 2.4. In this Chapter, we will see the results of this application. All the results regarding the analytical optimization have been produced with Python 3.10.8 installed on Ubuntu 23.04 for ARM® processor on a *virtual machine*. That one had 6 GB of available *RAM memory* and 6 CPU cores. For what regards, instead, the genetic algorithm, which is written in `C++`, it has been compiled with `CMake 3.24.3` and `GCC 12.2.0`.

5.1 Cross-sections, fluxes, and importances

To understand completely how the cross-sections change during the time and the flux and the importances are distributed in the core, it is useful to visualize the results of the preprocessing phase.

5.1.1 Cross-section

Each set of cross-section has been appropriately weighted on fluxes and importances in order to be used to compute either the power functional or the reactivity one. Figure 5.1 shows the cross-sections of absorption and fission for one of the elements with lower enrichment for BoC and EoC, after the weighting, as a function of in-core residence time. In particular, these cross-sections have been weighed on the generalized importance to the power functional at BoC, and thus used to compute the variation of this functional.

To have an idea on how the other cross-sections behave in function of the time and how the inner and outer region of enrichment differ, it is possible to look at the Appendix B.

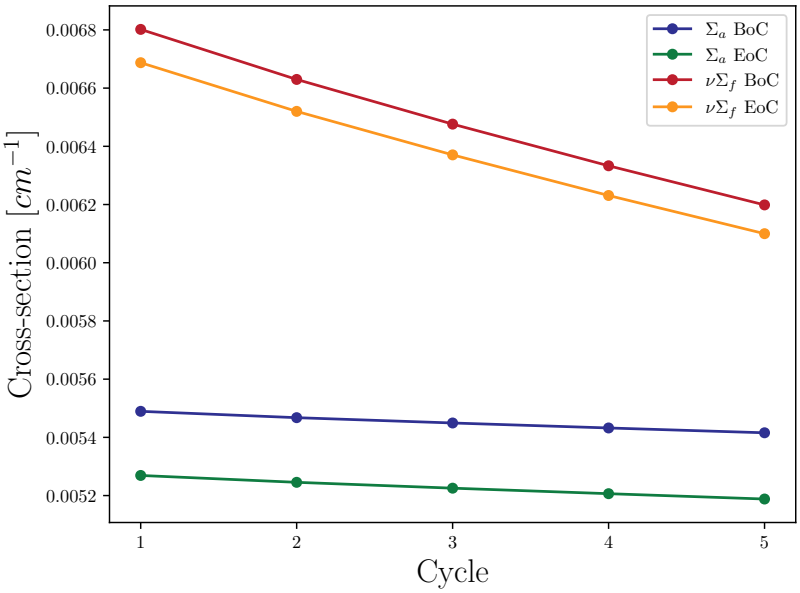

Figure 5.1. Cross-section of absorption and fission evolution for an element of the inner region, weighted to be used in the functional of the power.

5.1.2 Flux

We have already seen that because of the reactor geometry and the neutron transport equation, the flux is peaked around the center of the reactor. In the Figure 5.2 are reported the maps of the fuel assemblies, colored according to the neutron flux, for the reference states of BoC and EoC, that is the case in which all the fuel assemblies belong to the same batch. In Figure 5.2a it is clearly possible to observe the shape of the flux at BoC. The fuel assemblies in which the flux is higher are certainly the six around the central assembly, while the ones less irradiated by the neutrons are the external ones, at the boundaries with the inert materials. In this situation, it resulted a neutron multiplication factor $k_0 = 1.04532$.

The most interesting thing is to see how the flux evolves from BoC to EoC (Figure 5.2b). In that second image, we have a totally different situation. Indeed, we can firstly notice that the most irradiated fuel assemblies are not the 6 central ones anymore, but the peak has moved towards the core periphery. In addition, the peak has a lower intensity, as we can see from the scales of colors. Lastly, the outermost part has an increased neutron flux, as the control rods, which are extracted from the active region, now cannot capture neutrons in that region. In case of the reference EoC, since the fuel is still fresh but the control rods are not present in the active region, the neutron multiplication factor has a value of $k_0 = 1.06938$.

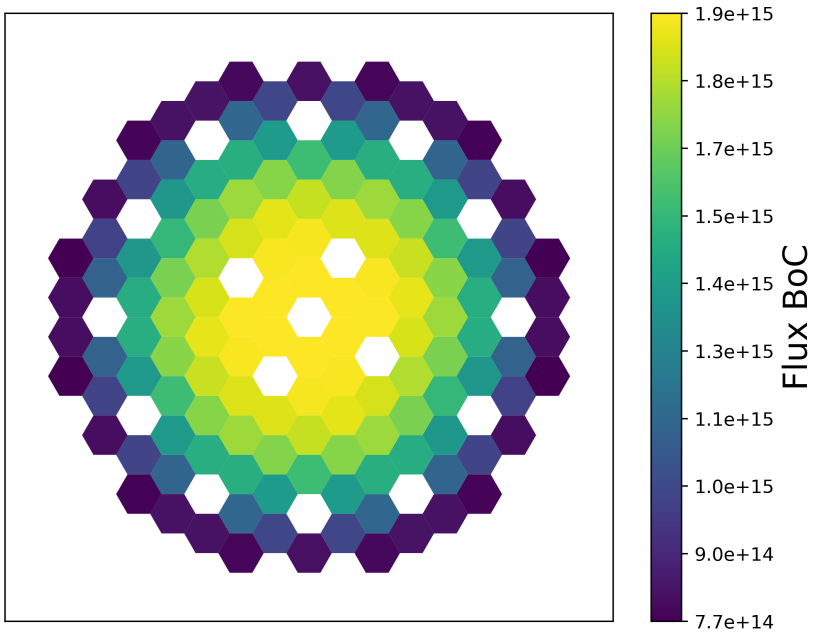

(a)

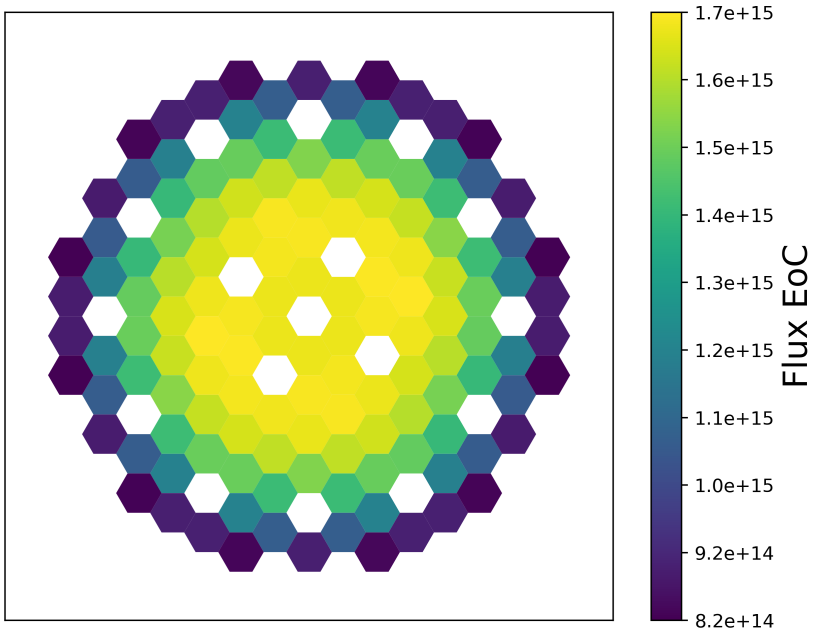

(b)

Figure 5.2. Flux distribution at BoC (Figure 5.2a) and at EoC (Figure 5.2b) of the reference state in which all the fuel assemblies belong to the same batch of the ALFRED reactor. The fluxes are measured in $[L^{-2}]$ $[T^{-1}]$.

5.1.3 Importance

Basically, for the importance (Figure 5.3a for BoC and Figure 5.3b for EoC) we can make the same consideration we have made about the flux. Indeed, in the case of ALFRED, the importance has the same behavior as the flux.

5.1.4 Generalized Importance

Concerning the generalized importance, in particular for the functional related to the power distribution of the Equation 3.24, we have several differences. In Figure 5.4 are reported the generalized importance for that functional at BoC and EoC. Considering the first case (Figure 5.4a) the most evident thing is that the six central fuel assemblies have the highest importance while the other ones' importance decreases moving away from the center, up to a negative value close to the outermost ring of control rods. This distribution can be understood by remembering the definition of the importance. The generalized importance is how much a neutron in a certain position contributes to a determined functional. In that case, the functional is the total power of the six central fuel assemblies, thus it is clear that a neutron positioned in one of these reference assemblies has the maximum importance. For the same reason, moving away from these reference assemblies decreases the neutron importance to the power peak.

If a region has a negative importance, it means that a neutron in that position reduces the power peak of the reference assemblies. This can be explained with the fact that the total power of the reactor is fixed. Indeed, a neutron positioned in a region far from the reference assemblies will probably fission around its position. This will produce some power and, since the total power is fixed, it will decrease in other parts of the core and, in particular, also in the reference assemblies.

The same thing happens at EoC (Figure 5.4b). Now, the reference assemblies are not anymore the central ones, but the yellow ones identified in the Figure. Indeed, due to the reactor design, we expect the fuel assembly with the highest power to be one of these. In this case, the assemblies with a negative importance are the ones at the center of the reactor.

5.2 Perturbation theory verification

Before showing the results of the optimizations, it is useful to see the goodness of our model for what regards the perturbation theory. In order to do that, we have

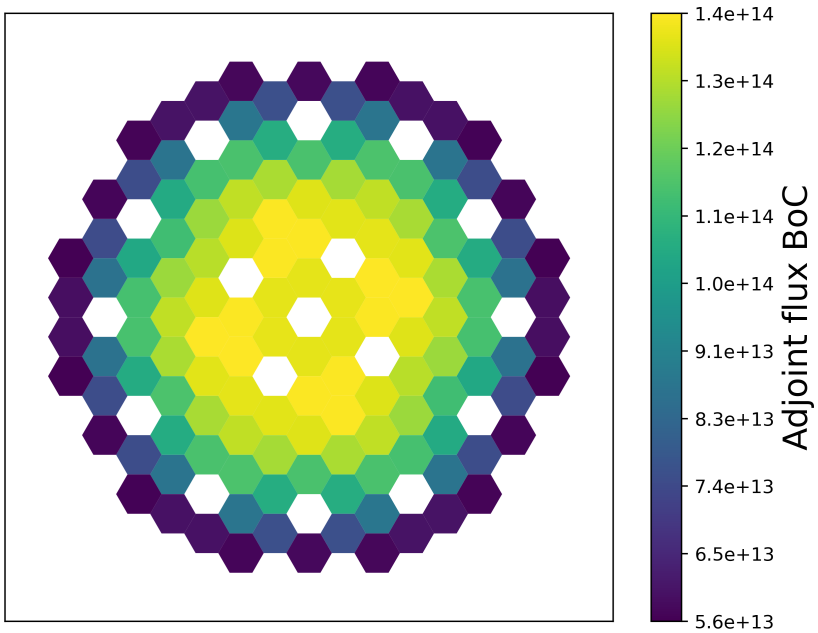

(a)

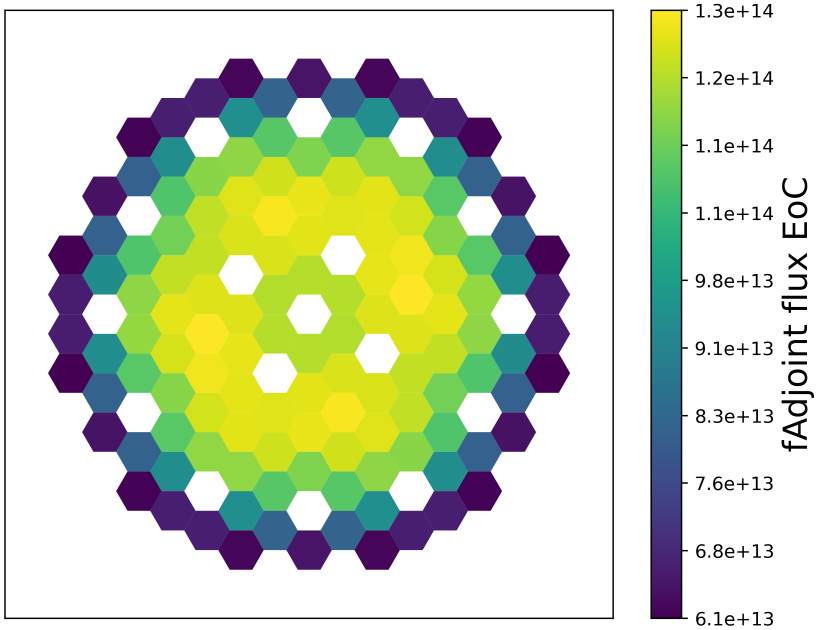

(b)

Figure 5.3. Importance distribution at BoC (Figure 5.3a) and at EoC (Figure 5.3b) of the reference state in which all the fuel assemblies belong to the same batch of the ALFRED reactor. The scale of values is in arbitrary units.

compared the result of the variation of the reactivity and of the functional of the power of a distribution with the exact (i.e. without using perturbation theory) static simulation of the system made with ERANOS. The distribution used to perform

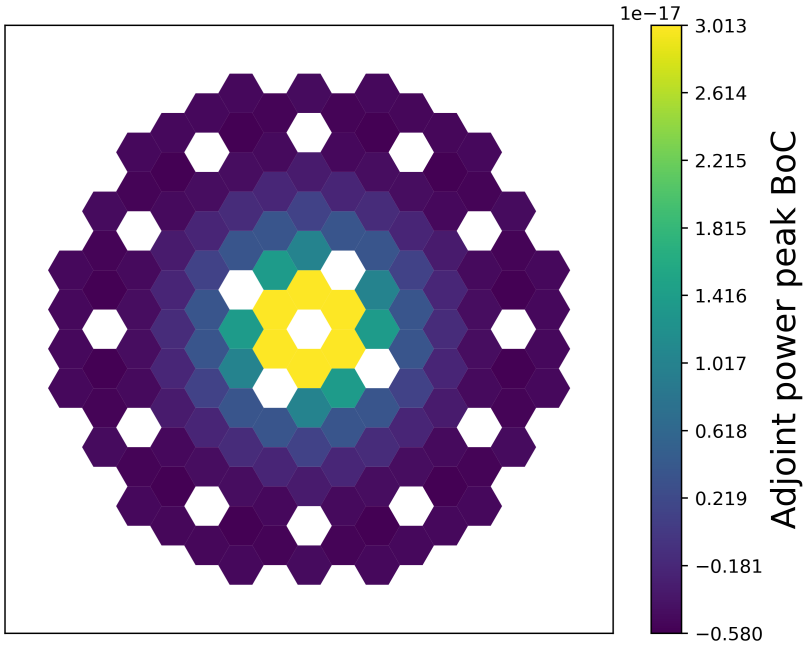

(a)

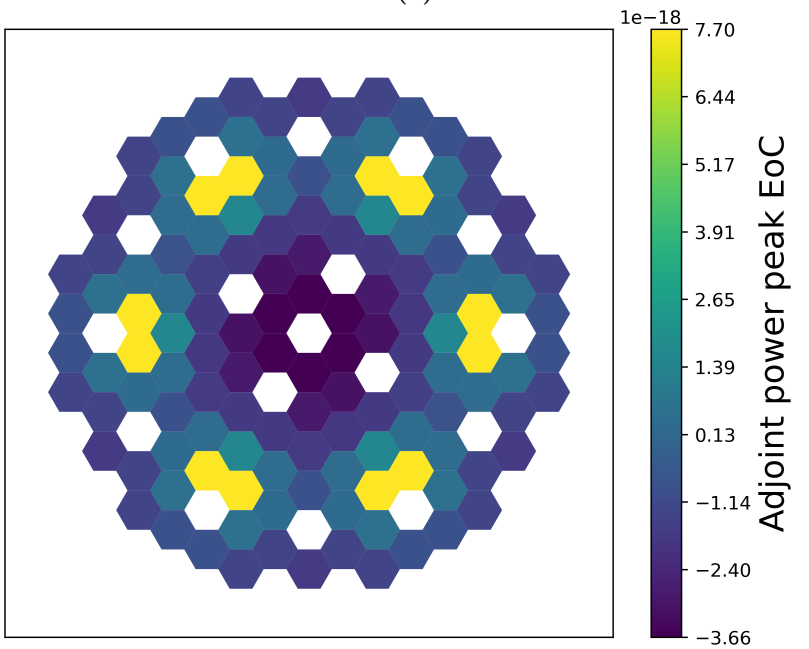

(b)

Figure 5.4. Generalized importance distribution at BoC (Figure 5.4a) and at EoC (Figure 5.4b) of the reference state in which all the fuel assemblies belong to the same batch of the ALFRED reactor. The scale of values is in arbitrary units.

this comparison comes from one of the experiment made during the developing of the algorithm and it is represented in Figure 5.5. Each color corresponds to a batch, i.e. to a spent-time in the core. In particular, for the cycle number one, the batch

number one is fresh at BoC and is one year old at EoC, the batch number two has spent one year inside at BoC and two years at EoC, and so on.

In Table 5.1 we reported the variation of the reactivity and the functional of the power for the distribution predicted from the model and the expected result from the exact simulation. If we look at the single values of the model and of the exact simulation, we notice that there is a large difference between them. In reality, this is not an issue for our model; indeed, we have set requirements not on the absolute value of the variations, but on the variation difference between the cycles. In particular, since the fitness function optimizes the standard deviations of the variations between the cycles, it is important that the obtained standard deviations are similar to the expected one. This is pretty well achieved, above all at EoC. The same thing can be seen from the Figure 5.6 and Figure 5.7, in which are reported the deviation from the average value of the variation of the two functional for the obtained result and for the simulation with ERANOS. In particular, we notice that at EoC the behavior of the two plot is almost identical, while at BoC this is not true, in particular for the power functional. The model at EoC is more in agreement with the simulation because the control rods, that are inserted just at BoC, introduce in the system correlation space-energy. Indeed, the control rods, that absorb mostly the slower neutrons, make the spectrum of energy near them harder (i.e. with a higher average energy). Therefore, the approximation we have made integrating separately the fluxes and the cross-sections is less valid with respect to BoC. It is important to notice that, even if the predicted behavior is not as expected, we have that the absolute difference in the standard deviations is acceptable.

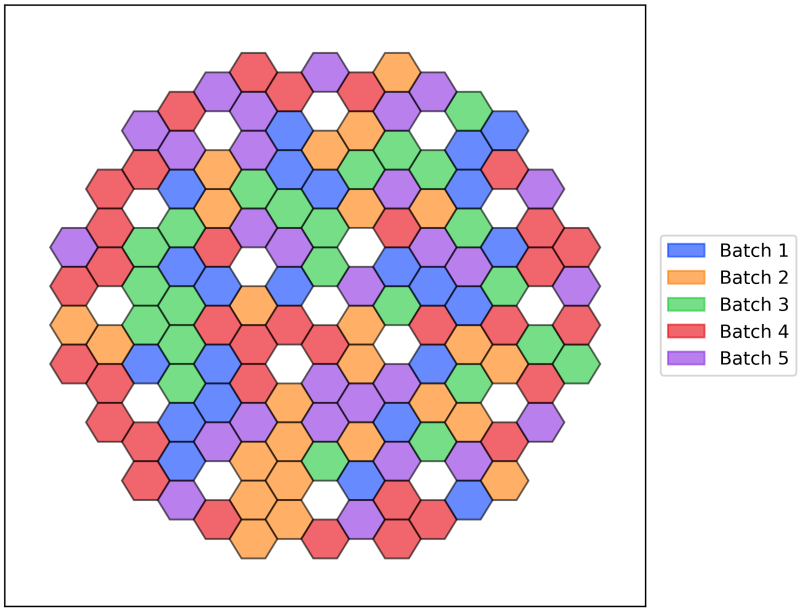

Figure 5.5. Batch distribution used to show the performances for what regards the perturbation theory.

Cycle	$\delta\rho$ [pcm]				$\delta\frac{\Delta P}{P}$ [%]			
	BoC		EoC		BoC		EoC	
	Model	Exact	Model	Exact	Model	Exact	Model	Exact
1	-3653	-4186	-5454	-6245	1.826	2.361	-1.560	-1.905
2	-3637	-4151	-5448	-6222	1.584	2.408	-0.924	-1.174
3	-3586	-4115	-5331	-6124	1.661	2.040	-4.236	-4.611
4	-3614	-4121	-5372	-6143	1.775	2.009	1.259	1.329
5	-3626	-4155	-5401	-6191	1.804	2.328	0.948	0.812
σ	25	29	52	51	0.10	0.19	2.22	2.37

Table 5.1. Comparison of the results obtained with the model described in the previous Chapter and the exact simulation.

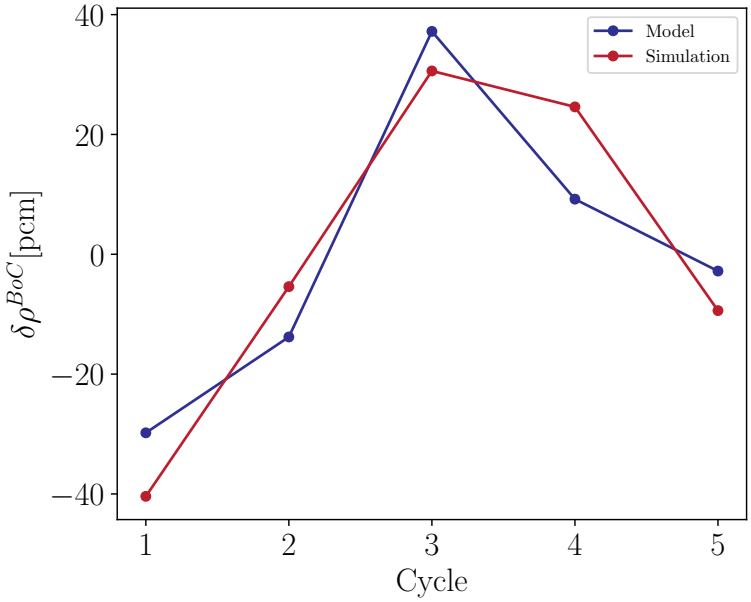

(a)

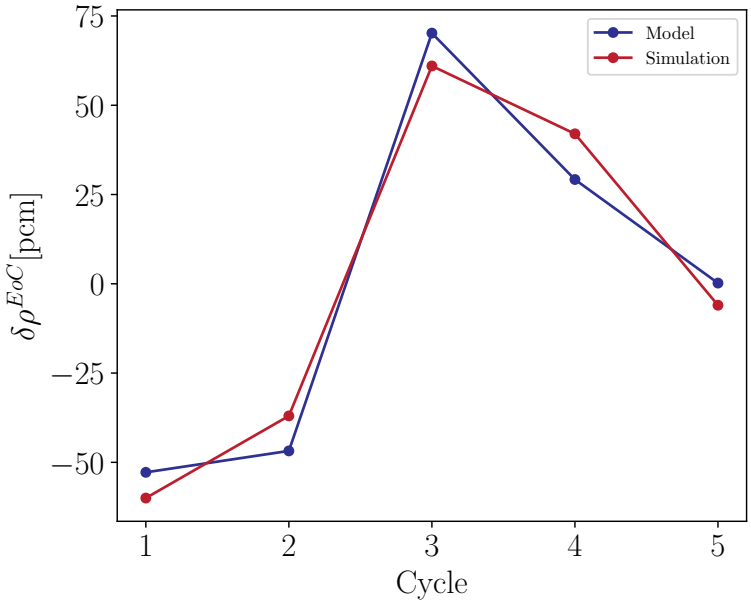

(b)

Figure 5.6. Deviation from the average of the reactivity variation between the cycle of the *test distribution* with the ERANOS simulation at BoC (Figure 5.6a) and EoC (Figure 5.6b).

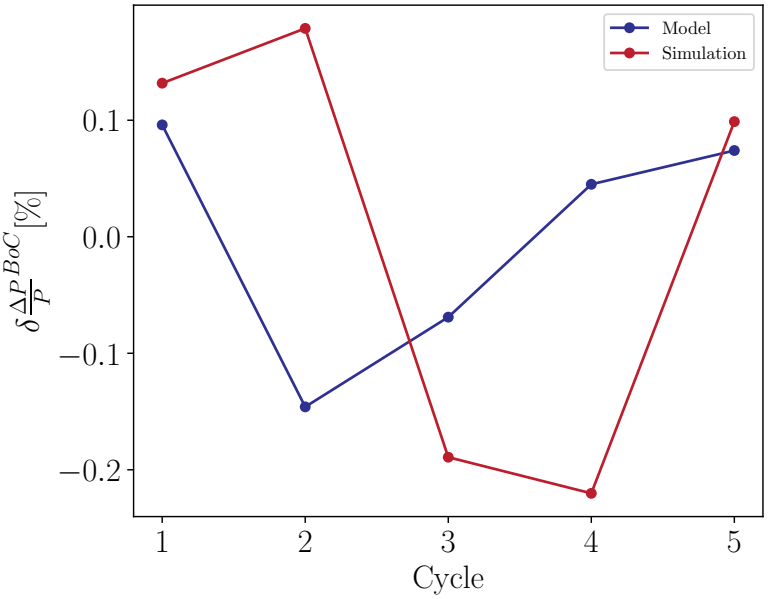

(a)

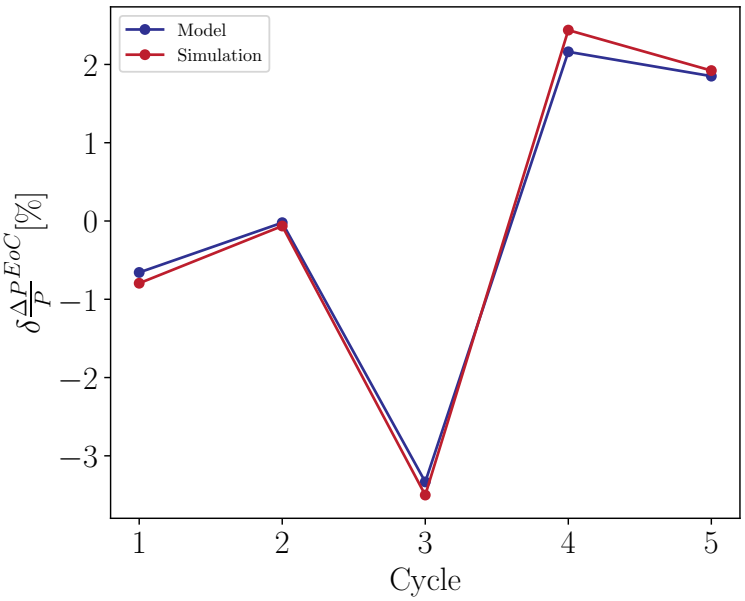

(b)

Figure 5.7. Deviation from the average of the variation of the power functional between the cycle of the *test distribution* with the ERANOS simulation at BoC (Figure 5.7a) and EoC (Figure 5.7b).

5.3 Analytical Algorithm

The analytical optimization part of the algorithm described in the previous Chapter was implemented using the Pyomo toolbox and, in particular, the *Mixed Integer Non-linear Decomposition Toolbox in Pyomo* (MindtPy) solver.

Since the numbers involved in the optimization can be very low, the Pyomo toolbox could have some numerical problems, in particular in the convergence to the solution. For this reason, it was necessary to introduce a multiplicative factor that multiplies all the terms of the Equation 3.25. It was chosen the value of 10^3. Consequently, the desired *absolute tolerance* to be reached between the upper and lower bound was scaled accordingly and set to 10^{-3}. The scaling factors that multiply each term of the fit function have been set at 0.5 each. The *relative bound tolerance*[1] was set to 10^{-7}. The other termination conditions we have set were the time limit to 3600 s, an iteration limit of 200 and a *stalling limit*[2] of 15 iterations. For the NLP sub-problems it has been used the `ipopt` solver, while for the MIP ones, the `gurobi persistent`. All the solvers exploited all the 6 cores of the machine.

5.3.1 Fuel assemblies distribution

With the setting above described, the optimization algorithm found a valid distribution in about 120 s[3] and obtained a fit-function value of $1.93248 \cdot 10^{-4}$. Consequently, the reason of exit from the optimization was the satisfaction of the absolute bound tolerance requirement. The corresponding assemblies distribution is the one represented in Figure 5.8. We can see that the fuel assemblies are distributed quite homogeneously in the core. Some clusters of elements belonging to the same batch are present, but their presence is in agreement with the type of fitness function used because we do not have asked for a homogeneous distribution. Based on qualitative considerations, we have to consider how much the functional we have chosen is representative of the functional we would like to use. For the reference assemblies for the power at BoC, the representativity of the functional used is high, indeed minimizing the power functional produce good results also for the single values of the power of the six assemblies. Instead, for the reference assemblies at EoC, the representativity decrease. This fact could be explained considering that the degrees of freedom (i.e. the difference between the number of assemblies involved and the

[1] Relative distance between the upper and lower bound.

[2] Maximum number of iterations without progress in the upper bound value.

[3] This time does not include the reading of the files and the preprocessing phase, that take about 30 s.

number of constraints) of the system for the sum of the six central fuel assemblies' powers are much less compared to the ones of the twelve assemblies taken as reference for the power at EoC.

The six central fuel assemblies are distributed as uniformly as possible between the batches, as expected. That means that five of them belong to a different batch each, while the remaining one has to be assigned to a batch that contains already one of the six elements. For the external twelve reference assemblies, instead, there are much more combinations.

In Table 5.2 it is possible to see how many assemblies there are for each batch and how they are distributed between the inner and outer zone of the core. While the first, second and fourth batches have the same cardinality, the third and fifth batches have slightly more assemblies. It is important to remember that for ALFRED it is not possible to obtain the batches with the same number of assemblies, because their number is not divisible by 5. While the inner fuel assemblies are distributed homogeneously within the five batches (except for the fourth batch), we find that for the external ones that is not true. We do not expect batches with the same cardinality because this request is not embedded in the fitness function. The only thing that we can assume is that while for the inner assemblies, the optimality is given by the elements distributed homogeneously between the batches for the outermost ones, that could not be true. Indeed, since both the flux and importance at BoC are peaked in the center of the core, the optimization of this region is more weighted in the fitness function and thus its optimization is prioritized with respect to the rest of the core.

The results concerning the values of the variation of the reactivity and of the functional of the power are summarized in Table 5.3. For the reactivity, we notice firstly the signs of the variations with respect to the reference states. Both the BoC and EoC reference states contain fresh fuel only, while the actual distribution includes both fresh and burned fuel assemblies. Since the fuel burning results in a reduction of the number of fissile atoms available, the cross-sections variations with respect to the reference states are negative or null (see Figure 5.1). Therefore, the reactivity variations are also negative. We notice also that the standard deviation of the variation of the reactivity is within 20 pcm, that is well below the threshold that can be, in general, considered the sensitivity we are able to measure and that does not influence the reactor design, that is about 100 pcm. Regarding the variation of the power functional, we have still very good results: the standard deviation is below 0.02% for both BoC and EoC. In this case, the reference value can be considered

Batch	1	2	3	4	5
Internal	11	11	11	12	11
External	13	13	18	12	22
n° of FA	24	24	29	24	33

Table 5.2. Cardinality of each batch for the distribution obtained with the analytical algorithm.

as not affecting the reactor design if the batches introduce a penalty negligible with respect to the natural variation due to the burning of the fuel. These values correspond to 0.5% for BoC and 0.1% for EoC. The difference between BoC and EoC lays in the fact that the functional is different: at BoC we have 6 elements as reference, while at EoC 12.

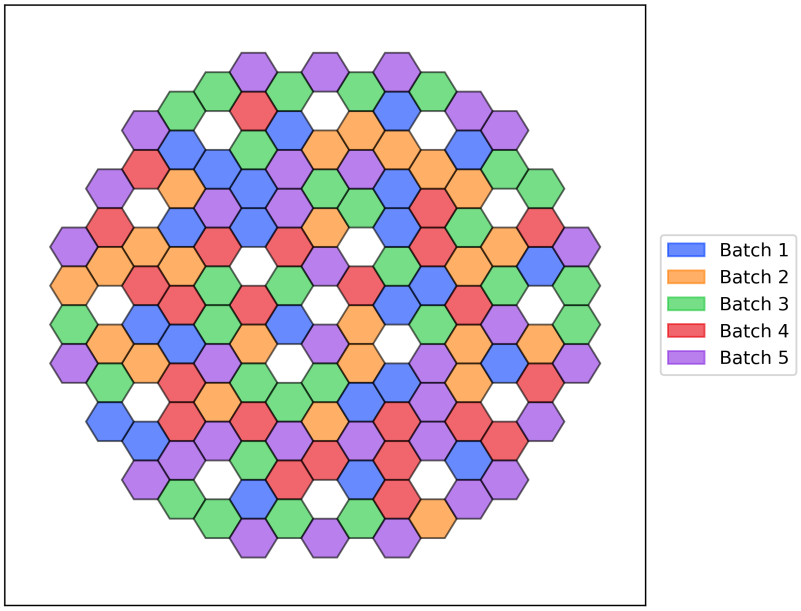

Figure 5.8. Distribution of fuel assemblies in batches for the test-case ALFRED, found with the analytical optimization.

5.3.2 Evolution of the solution

The solution is obtained, after the relaxed NLP, in two complete iterations, that include the MILP, the regularization and the NLP. The best value of the fitness function obtainable with the relaxed NLP is of $-8.72083 \cdot 10^{-94}$ while in the two NLP iterations, we obtain respectively 2.41146 and $1.93241 \cdot 10^{-4}$, that is the value

[4]This value is smaller than the convergence threshold chosen. Thus, it can be considered 0.

Cycle	$\delta\rho$ [pcm]		$\delta\frac{\Delta P}{P}$ [%]	
	BoC	EoC	BoC	EoC
1	-3625.4	-5413.3	1.7397	-0.8952
2	-3605.5	-5375.8	1.7194	-0.9012
3	-3647.3	-5421.1	1.7333	-0.8956
4	-3620.4	-5402.1	1.7530	-0.9069
5	-3617.4	-5393.3	1.7038	-0.9133
σ	15.3	17.7	0.0189	0.0077

Table 5.3. Variations of the reactivity and of the functional of the power with respect to the unperturbed state in the five cycles, at BoC and EoC, of the distribution find with the analytical algorithm. In the last line, it is reported the standard deviation of the variation between the cycles.

that satisfies the termination condition.

5.4 Genetic Algorithm

To make a fair comparison with the results obtained with the analytical optimization, we use the same fitness function, with the same normalization and scaling factors as in the algorithm showed above.

The results obtained with the genetic algorithm have been generated with the following parameters of configuration. For each *generation*, there are 80 *individuals*. The number of *tournaments* is 7 and the probability ratio p (Section 4.3) is 0.3. The probability of *crossing-over* and *mutation* on the whole generation are respectively of 0.8 and 0.5. For each iteration, the 0.1% of the best *individuals* are passed to the next *generation* without being crossed with other *individuals*.

Concerning the termination condition, it is possible to use a limit on the time, the number of generations, the best fitness function value or on the average fitness function value of the generation. As in the analytical optimization, we have used the condition on the fitness value to be reached, of 10^{-3}.

The genetic algorithm has a random nature, since the number of mutations and their position is aleatory. For this reason, the results depend on the chosen seed of the pseudo-random generator.

5.4.1 Fuel assemblies distribution

The results obtained were generated in about 1070 s and in about 560 generations, and the distribution found has a fitness function of $8.81286 \cdot 10^{-4}$. The obtained

Batch	1	2	3	4	5
Internal	6	12	13	10	15
External	24	12	12	19	11
n° of FA	30	24	25	29	26

Table 5.4. Cardinality of each batch for the distribution obtained with the genetic algorithm.

distribution is reported in Figure 5.9. We can see that the fuel assemblies are pretty well distributed among the core map, even if there are four small clusters of three of elements belonging to the same batch.

Also in this case, the central assemblies are distributed as homogeneously as possible between the five batches, resulting in the first batch containing two elements of this type.

The fuel assemblies are divided between the batches according to the Table 5.4, therefore there is just six assemblies of difference between the most populated batch and the less populated one. Looking at the allocation of the assemblies between the two types of enrichment, we notice that, while in the second batch the number of fuel assemblies in the inner region is identical to the one in the periphery of the core, in the first batch we have a big difference of 18 assemblies. This imbalance is probably due to the fact that once in the inner region there are few assemblies, it is necessary to increase the number in the external region to make the reactivity variation similar between the cycles. This big imbalance does not recur in any other batch.

Instead, the values of the variation of the reactivity and of the power functional are reported in Table 5.5. Also in that case, we can see that the standard deviation of the reactivity variation between the cycles is below 100 pcm, that can be considered, in general, a threshold below which the result can be considered good and that does not affect the design of the reactivity control system. Even for the power, the variations are small compared to the indicative reference values introduced in the previous Section of 0.5% for BoC and 0.1% for EoC, thus also in that case the result is good.

5.4.2 Evolution of the solution

The genetic algorithm provides us in output a series of information. The most relevant ones are the plot that describes the evolution of the fitness function in function of the generation, and the number of new individuals per generation that

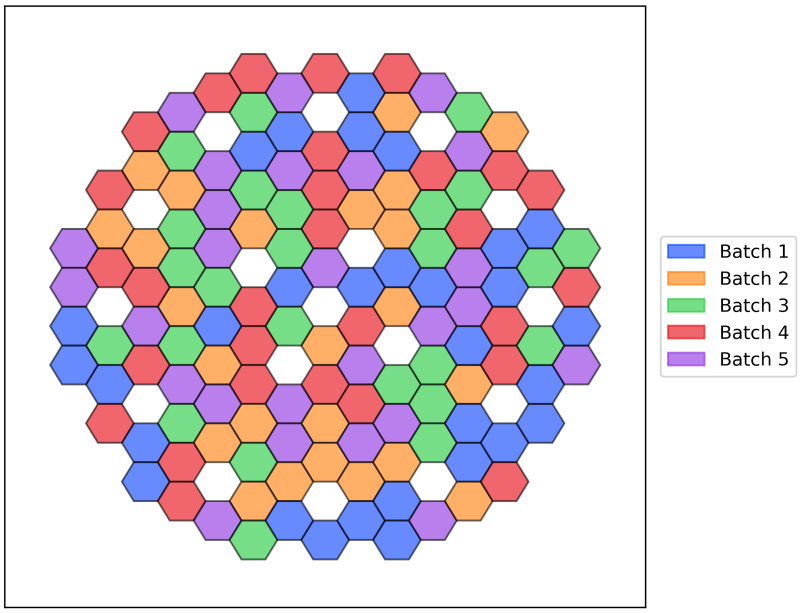

Figure 5.9. Distribution of fuel assemblies in batches for the test-case ALFRED, found with the genetic optimization.

Cycle	$\delta\rho$ [pcm]		$\delta\frac{\Delta P}{P}$ [%]	
	BoC	EoC	BoC	EoC
1	-3593.6	-5334.3	1.7254	-0.8685
2	-3650.7	-5425.8	1.6931	-0.9105
3	-3625.9	-5394.5	1.7693	-0.8735
4	-3616.8	-5410.4	1.7075	-0.9017
5	-3629.1	-5440.6	1.7538	-0.9580
σ	20.7	41.1	0.0316	0.0358

Table 5.5. Variations of the reactivity and of the functional of the power with respect to the unperturbed state in the five cycles, at BoC and EoC, of the distribution find with the genetic algorithm. In the last line, it is reported the standard deviation of the variation between the cycles.

have never been met in all the past (that is in the previous generations). The first plot can be found in Figure 5.10. Here, the value of the best fitness function in the generation and the evolution of best fitness function average are reported. This allows to understand that at the beginning the fitness function decreases very rapidly and then slows down. The second curve, regarding the best average fitness function values of the population, helps us to understand if and how the population is evolving. In the case this curve is too constant and does not decrease, it means that population statistically is always the same, and there are no improvement inside it. If it stays very close to the best fitness function (i.e. the other line in the Figure), it means that there could be a homogenization of the population: therefore the possibilities of gene recombination are low and the capability of the algorithm of finding new solutions is reduced. Thus, it is necessary to have a balance between these two factors.

Running the optimization for a smaller amount of time or requiring a bigger target value for the convergence could lead to obtain acceptable results, i.e. within the limits we talked in Section 5.3.1, in a smaller amount of computational time.

The other plot can be found instead in the Figure 5.11. Having an idea of how many new individuals the algorithm is searching each generation can be helpful to understand if it is necessary to introduce more mutation or crossing over or reduce the elitism. Generally, increasing the number of new individuals per each generation also increases the CPU-time per each generation. Indeed, since the fitness function value of each encountered individual is stored in memory and that the computational time of the fitness is the most time-consuming operation, more new individuals to compute result in longer processing time.

5.5 Comparison between the analytical and genetic approaches

Both analytical and genetic optimization techniques have produced promising results, demonstrating the potential to generate a fuel assembly distribution into batches that aligns with the reactor design requirements, without compromising its safety.

Comparing the batch distributions (Figure 5.8 and Figure 5.9) we can see that the analytical one is more homogeneous, while the genetic one has some more clusters. The fitness function values reached in these two cases are respectively of $1.93248 \cdot 10^4$ and $8.81286 \cdot 10^4$. In general, we have obtained better results with

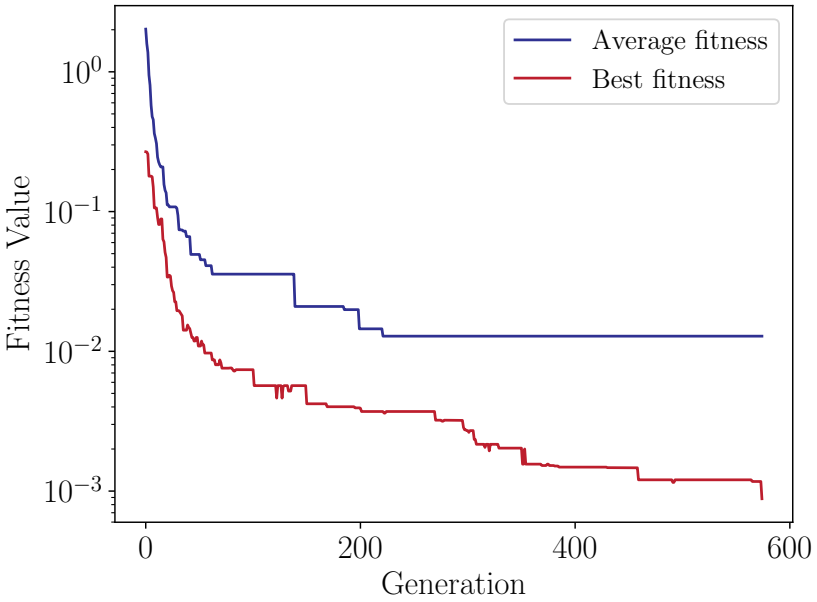

Figure 5.10. Evolution of the best fitness function value found in each generation (red) and the best average fitness from the beginning of the evolution (blue).

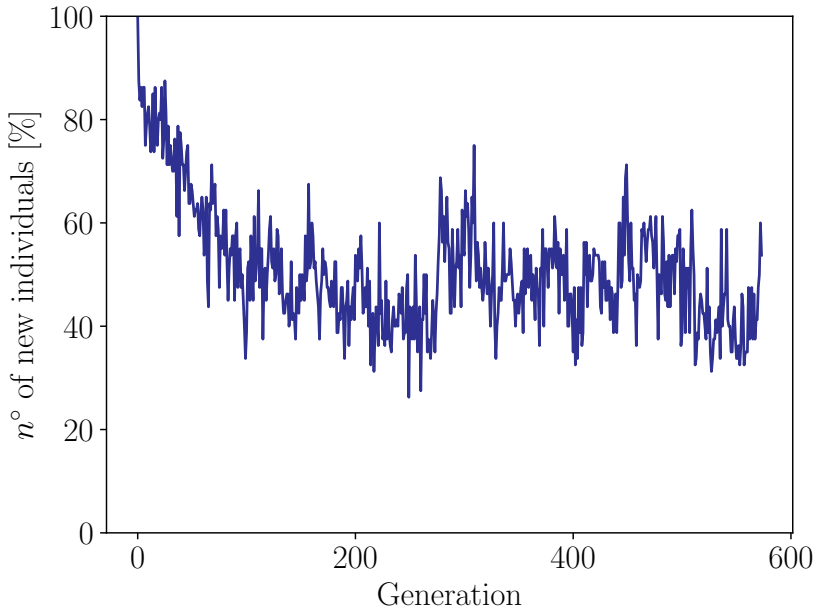

Figure 5.11. Percentage of new individuals with respect to the population in function of the generation.

the analytical algorithm rather than the genetic one, both in terms of the fitness function obtained and of the computational time needed to achieve the distribution. This does not mean that the genetic algorithm is in general worse with respect to the analytical one. Indeed, the fit function used in this work of thesis has a relatively simple shape, but for a more complex expression, that could include other terms, the computational time can be higher. The computation of all the gradients of the *outer approximation*, resulting from the various linearizations needed and the regularization process, can be more time-consuming with respect to the operations needed in the genetic algorithm. Therefore, in that case, the analytical algorithm would result in a worse choice with respect to the genetic one.

In addition, the fact that the genetic algorithm computes the fitness function in Python and performs the other operation in `C++` (Chapter 4) could have further slowed the process. Thus, we can probably say that the better choice of the optimization algorithm is problem-dependent, because there are many factors that can make an algorithm a better choice with respect to the other one.

Chapter 6

Conclusion and Future Activities

The development of an algorithm that helps finding a batch distribution that meets the reactivity and power distribution requirements is a key part of the reactor design. While for thermal reactors some tools already exists, for innovative reactors such as the lead-cooled ones, no standard tool exists so that finding a good batch distribution was made by *trial and fail* and required many days. The two developed algorithms, i.e. the analytical and the genetic one, which employ the perturbation theory to drastically reduce the computational time to the order of the hundreds of seconds, return good outcomes. The former solves the problem with the *Mixed Integer Non-Linear Programming*, while the second one exploits some procedures related to the theory of evolution of a population.

In general, for the specific problem we have solved, that is the test-case of the *Advanced Lead-cooled Fast Reactor European Demonstrator* (ALFRED), we have obtained better results with the analytical algorithm, both in terms of the uniformity of the batch distribution, and therefore in terms of the fitness function, and in terms of computational time that resulted a bit shorter. However, it is important to note that we could be in a different situation for a different fitness function, especially for more complicated ones.

Despite that the obtained results are in agreement with the expected results from the full simulation of the system with ERANOS, there is the possibility to improve the quality of the results. For time reason and to keep the model simple as a first step, these possibilities have not been explored during the internship, but they will be briefly presented.

The most important approximation that can be relaxed is the one regarding the definition of the generalized importance for the power functional. We have defined it as the contribution of one neutron to the functional $\Delta P/P$, with P representing the contribution of the *reference assemblies* to the total reactor power. The best theoretical model (Section 5.1.4) would take as reference assembly the hottest one, but it is impossible to know a priori which assembly it is. Thus, we could consider all the fuel assemblies, but it would require the importances of all the assemblies and much time to compute the corresponding fitness function. For this reason, as *reference assemblies* for the test-case of ALFRED, we have taken the six central assemblies at BoC and the twelve ones next to the external control rods at EoC. This is an approximation because we actually aim at minimizing the temperature of the hottest assembly and not the sum of the temperature of the reference assemblies. This approximation could be relaxed using the generalized importance of each single assembly among those which we expect to be the hottest ones.

Another very important point to be improved is the *correlation space-energy* approximation. As we have said in Section 3.6.2, we have performed the volume and energy integrals in two different steps. This allowed to compress the three-dimensional fluxes and importances to a two-dimensional field before the computation of the new set of cross-sections. This is not correct from a mathematical point of view, but it works pretty well from a practical one. The results can be further improved by taking into account the effect of the integrals and create the new set of cross-sections of each element by weighing on the flux and importance of each axial cell, as well as on the energy. This will not produce relevant differences in the standard deviation of the results, that is a measure of the variability between the cycles, but it will improve the absolute value of the variations.

In addition, to improve the quality of the obtained distribution, it is possible to include other terms in the fitness function that take into account other phenomena that occur in the reactor. For example, it is possible to introduce another term that concerns the *anti-reactivity worth* of the control rods. The *anti-reactivity* is the variation of the reactivity caused by the movement of the control rods and it partially depends on the fuel assemblies distribution. In this case, it must be ensured that in all cycles the *anti-reactivity worth* of the control rods is sufficient for safety purposes. Another possibility is to introduce other constraints that take into account also the *shuffling* of the position of the elements in the core between the cycles.

Further studies will be necessary to optimize the operation of the Pyomo solvers

and the model used, but the designed algorithms have produced very promising results and will be a very useful tool in the reactor design process.

Appendix A

Exploring the Pareto front

In multi-objective optimization, the Pareto front [31] is a set of optimal solutions. Specifically, it is composed by points that are optimal for one or more objectives but not simultaneously optimal for all objectives. In multi-objective optimization indeed, often it is not possible to find a single solution that is superior to all other solutions with respect to all objectives. Since, in general, an optimal solution for all the objectives does not exist, the Pareto front is useful in engineering to evaluate the goodness of a solution.

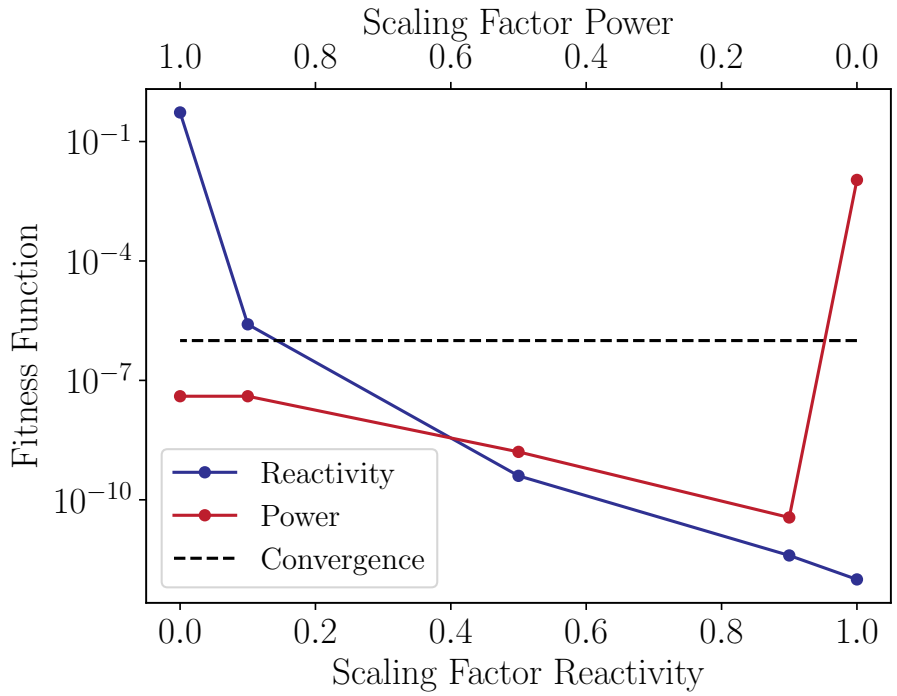

Figure A.1. Pareto front obtained by computing the optimization of the reactivity and power functional at BoC.

In our case, the problem consisted in the optimization of two objectives: the reactivity and the power distribution; therefore it was possible to explore the Pareto front by modifying the scaling factor for each functional of the fitness function.

This has been done with just the two functional at BoC, without optimizing at EoC. The results can be seen in Figure A.1. In the abscissae there are the scaling factors that multiply the terms regarding the reactivity (at the bottom) and the ones concerning the power of BoC. The scaling factors multiplying the EoC terms were set to 0. In the ordinate, it is present the value of the fitness function. In black, it is reported the convergence value below which the `Pyomo` algorithm was not able to distinguish anymore the values. This means that all the values below the black line, for the algorithm, are the same.

As we can see, three values are above the convergence line, while the other ones stay below. If we try to optimize both functionals, with any scaling factor, we obtain a solution in which both the values are below this line and so not distinguishable. In the presented result of the optimization, in the absence of a clear advantage for more complex combinations, we have chosen to give the same weight to both the reactivity and power functional, using 0.5 as scaling factors for both.

One important thing to remember is that the convergence condition is checked on the difference between upper and lower bound. Therefore, even if the points are above the convergence line, it does not mean that they have not converged to the solution.

Appendix B

Cross-sections plots

In the Section 3.5.2 we have showed that in the preprocessing phase, we have generated a new set of cross-sections, starting from the ones read in input. A new set of cross-sections has been created for each functional and for each fuel assembly. In the following Figures, we show how the cross-sections of absorption, fission and power change over years, for BoC and EoC and for a representative element of the innermost region and one of the outermost one.

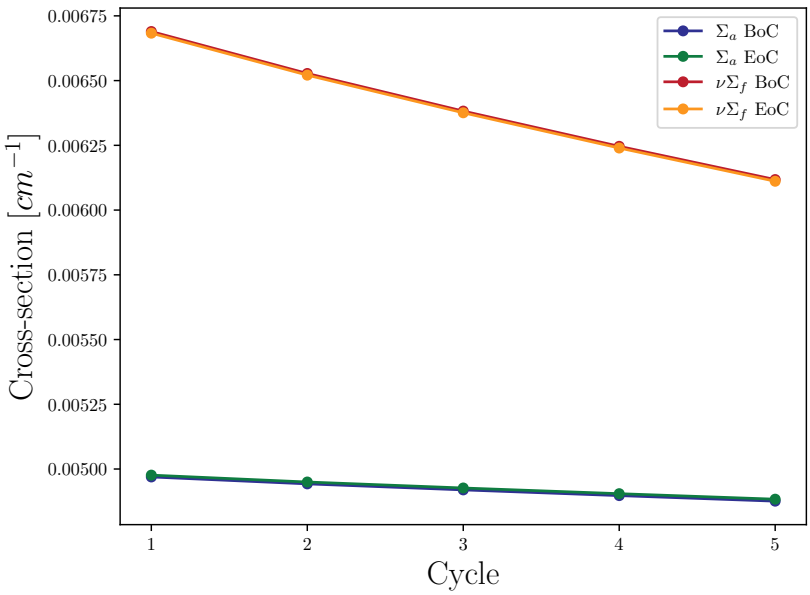

Figure B.1. Evolution of absorption and fission cross-section weighted on the flux and importance, at BoC and EoC for the innermost region, to be used in the computation of the reactivity functional.

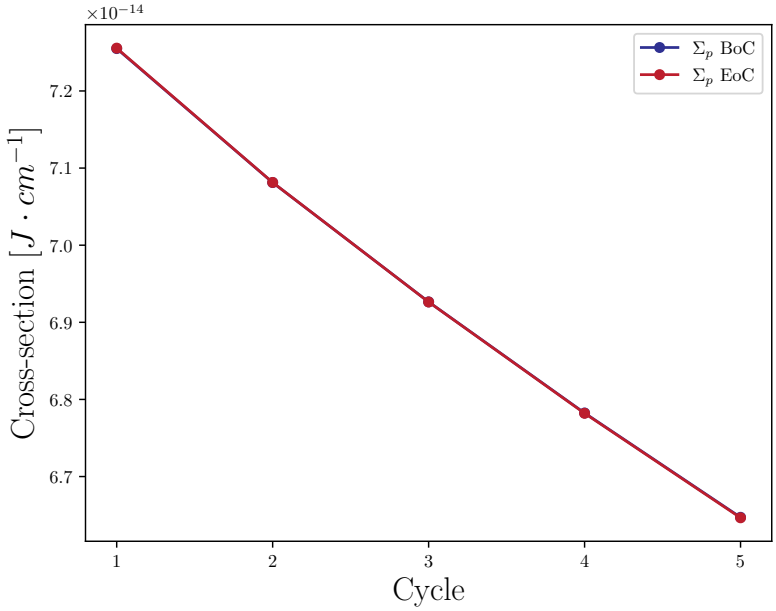

Figure B.2. Evolution of the power cross-section, at BoC and EoC, weighted on just the flux at BoC or EoC for an element of the innermost region.

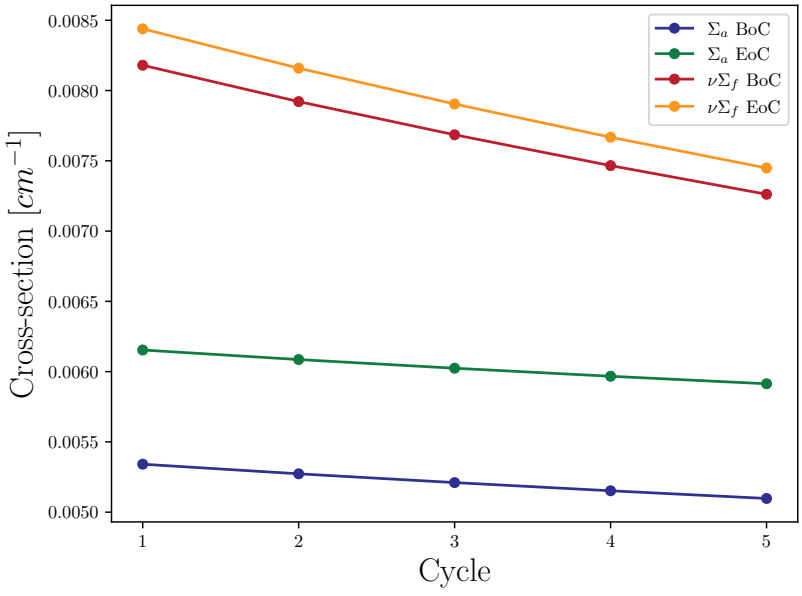

Figure B.3. Evolution of absorption and fission cross-section weighted on the flux and generalized importance, at BoC and EoC for the outermost region, to be used in the computation of the power functional.

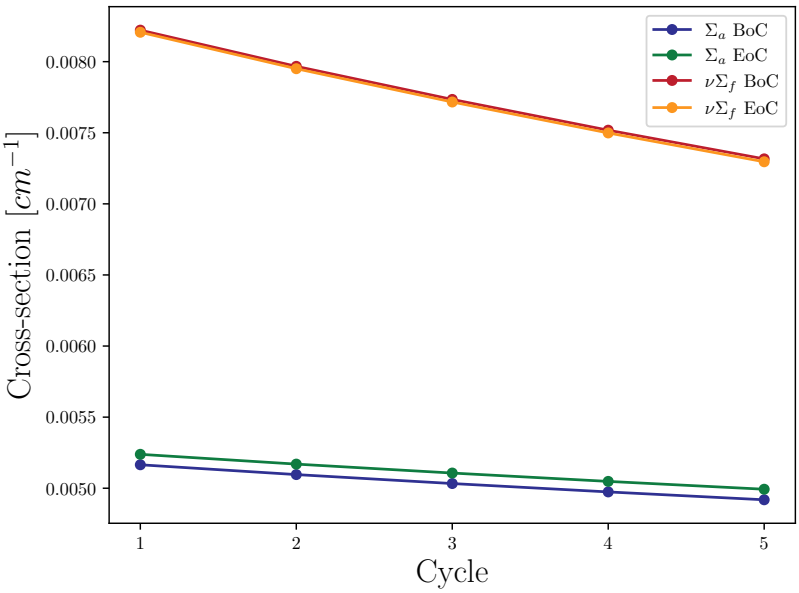

Figure B.4. Evolution of absorption and fission cross-section weighted on the flux and importance, at BoC and EoC for the outermost region, to be used in the computation of the reactivity functional.

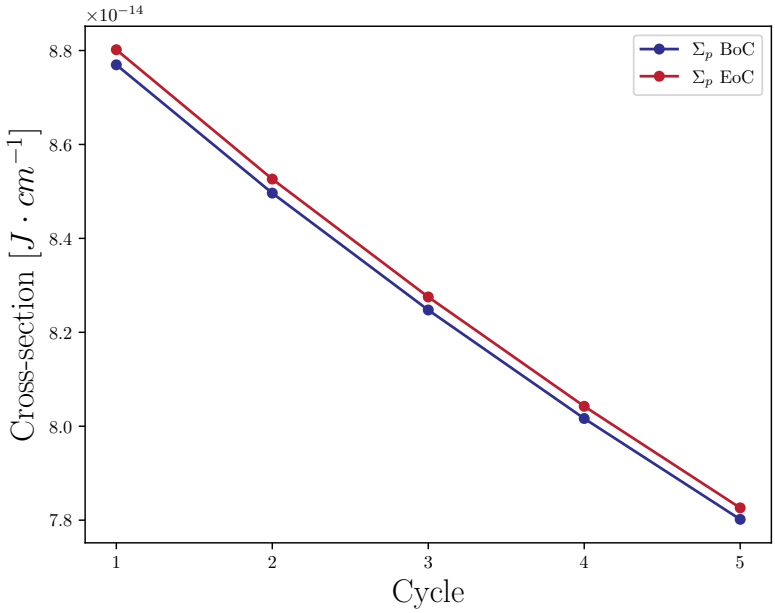

Figure B.5. Evolution of the power cross-section, at BoC and EoC, weighted on just the flux at BoC or EoC for an element of the outermost region.

Bibliography

[1] Max Roser and Lucas Rodés-Guirao. "Future Population Growth". In: *Our World in Data* (2013). URL: https://ourworldindata.org/future-population-growth.

[2] Graham Zabel. *The Interrelationship between Population Growth and Energy Resources*. 2009. URL: https://www.resilience.org/stories/2009-04-20/peak-people-interrelationship-between-population-growth-and-energy-resources/#:~:text=Growing%5C%20populations%5C%20consume%5C%20more%5C%20energy.%5C%20Availability%5C%20of%5C%20energy,has%5C%20to%5C%20be%5C%20drilled%5C%20in%5C%20more%5C%20complex%5C%20environments..

[3] Hannah Ritchie. "How does the land use of different electricity sources compare?" In: *Our World in Data* (2022). URL: https://ourworldindata.org/land-use-per-energy-source.

[4] *Technology Road-map Update for Generation IV Nuclear Energy Systems*. Jan. 2014. URL: https://www.gen-4.org/gif/upload/docs/application/pdf/2014-03/gif-tru2014.pdf.

[5] *Our common future*. en-US. Report. Transmitted to the General Assembly as an Annex to document A/42/427 - Development and International Co-operation: Environment. New York: World Commission on Environment and Development, Oct. 1987. URL: http://www.un-documents.net/wced-ocf.htm.

[6] Luminita Grancea, Mark Mihalasky, and Martin Fairclough. *Uranium 2020: Resources, Production and Demand. Red Book 2020*. Dec. 2020.

[7] United States Nuclear Regulatory Commission. *Glossary, Natural Uranium*. URL: https://www.nrc.gov/reading-rm/basic-ref/glossary/natural-uranium.html.

[8] *Fundamental Safety Principles*. Safety Fundamentals SF-1. Vienna: INTERNATIONAL ATOMIC ENERGY AGENCY, 2006. URL: https://www.iaea.org/publications/7592/fundamental-safety-principles.

[9] *Technical Features to Enhance Proliferation Resistance of Nuclear Energy Systems*. Nuclear Energy Series NF-T-4.5. Vienna: INTERNATIONAL ATOMIC ENERGY AGENCY, 2010. URL: https://www.iaea.org/publications/8418/technical-features-to-enhance-proliferation-resistance-of-nuclear-energy-systems.

[10] World Nuclear Association. *Generation IV Nuclear Reactors*. URL: https://world-nuclear.org/information-library/nuclear-fuel-cycle/nuclear-power-reactors/generation-iv-nuclear-reactors.aspx.

[11] Luciano Cinotti et al. "Lead-Cooled Fast Reactor (LFR) Design: Safety, Neutronics, Thermal Hydraulics, Structural Mechanics, Fuel, Core, and Plant Design". In: *Handbook of Nuclear Engineering*. Ed. by Dan Gabriel Cacuci. Boston, MA: Springer US, 2010, pp. 2749–2840. DOI: 10.1007/978-0-387-98149-9_23. URL: https://doi.org/10.1007/978-0-387-98149-9_23.

[12] 2006. URL: https://cordis.europa.eu/project/id/36439.

[13] J A Grundl. "FISSION-NEUTRON SPECTRA: MACROSCOPIC AND INTEGRAL RESULTS." In: (Oct. 1971). DOI: 10.2172/4754459. URL: https://www.osti.gov/biblio/4754459.

[14] Cross Section Evaluation Working Group. *ENDF/B-VI Summary Documentation*. 2011. URL: https://www.nndc.bnl.gov/sigma/index.jsp.

[15] "Toward an Integrated Nuclear Fuel Cycle". In: 1 (2008), pp. 24–32. URL: https://eprijournal.com/wp-content/uploads/2016/02/2008-Journal-No.-1.pdf.

[16] F. Lodi. *ALFRED Geometric Data for modelling*.

[17] Bell G. I. and Glasstone S. "Nuclear Reactor Theory". In: (Oct. 1970). URL: https://www.osti.gov/biblio/4074688.

[18] J. TOMMASI. *ERANOS USERS MANUAL APPLICATIONS OF PERTURBATION THEORY WITH FINITE DIFFERENCE DIFFUSION AND SN TRANSPORT FLUX SOLVERS*. Tech. rep. CEA.

[19] Nuclear Energy Agency - NEA. *ERANOS 2.3N*. URL: https://www.oecd-nea.org/tools/abstract/detail/nea-1683/.

[20] Michael L. Bynum et al. *Pyomo–optimization modeling in python*. Third. Vol. 67. Springer Science & Business Media, 2021.

[21] William E Hart, Jean-Paul Watson, and David L Woodruff. "Pyomo: modeling and solving mathematical programs in Python". In: *Mathematical Programming Computation* 3.3 (2011), pp. 219–260.

[22] Wenzel Jakob, Jason Rhinelander, and Dean Moldovan. *pybind11 – Seamless operability between C++11 and Python*. https://github.com/pybind/pybind11. 2017.

[23] D.A. Brown, M.B. Chadwick, R. Capote, et al. "ENDF/B-VIII.0: The 8^{th} Major Release of the Nuclear Reaction Data Library with CIELO-project Cross Sections, New Standards and Thermal Scattering Data". In: *Nuclear Data Sheets* 148 (2018). Special Issue on Nuclear Reaction Data, pp. 1–142. DOI: https://doi.org/10.1016/j.nds.2018.02.001. URL: https://www.sciencedirect.com/science/article/pii/S0090375218300206.

[24] *Salome platform*. URL: https://www.salome-platform.org.

[25] E. de Klerk et al. "Optimization of nuclear reactor reloading patterns". In: *Annals of Operations Research* 69.0 (1997), pp. 65–84. DOI: 10.1023/A:1018953616965. URL: https://doi.org/10.1023/A:1018953616965.

[26] Jan Kronqvist et al. "A review and comparison of solvers for convex MINLP". Odefinierat/okänt. In: *Optimization and Engineering* 20 (2019). ast., pp. 397–455. DOI: 10.1007/s11081-018-9411-8.

[27] Jan Kronqvist, David E. Bernal, and Ignacio E. Grossmann. "Using regularization and second order information in outer approximation for convex MINLP". In: *Mathematical Programming* 180.1 (2020), pp. 285–310. DOI: 10.1007/s10107-018-1356-3. URL: https://doi.org/10.1007/s10107-018-1356-3.

[28] Yongsheng Fang and Jun li. "A Review of Tournament Selection in Genetic Programming". In: Oct. 2010, pp. 181–192. DOI: 10.1007/978-3-642-16493-4_19.

[29] Mattia Massone. "CROSS-SECTIONS FOR TRANSIENT ANALYSES: DEVELOPMENT OF A GENETIC ALGORITHM FOR THE ENERGY MESHING". PhD thesis. Karlsruher Instituts fur Technologie (KIT), 2018.

[30] Wikimedia Commons. *File:OnePointCrossover.svg — Wikimedia Commons, the free media repository*. [Online; accessed 27-July-2023]. 2020. URL: https://commons.wikimedia.org/w/index.php?title=File:OnePointCrossover.svg&oldid=492531820.

[31] M. Akbari et al. "13 - Artificial neural network and optimization". In: *Advances in Friction-Stir Welding and Processing*. Ed. by Mohammad Kazem Besharati Givi and Parviz Asadi. Woodhead Publishing Series in Welding and Other Joining Technologies. Woodhead Publishing, 2014, pp. 543–599. DOI: https://doi.org/10.1533/9780857094551.543. URL: https://www.sciencedirect.com/science/article/pii/B9780857094544500136.